Thesis Proposal

Robust and Natural Gait via Neuromuscular Control for Tansfemoral Prostheses

Nitish Thatte
November 14, 2016

The Robotics Institute
Carnegie Mellon University
Pittsburgh, PA 15213

Thesis Committee:
Hartmut Geyer (Chair)
Steven Collins
Chris Atkson
Elliot Rouse, Northwestern University

Submitted in partial fulfillment of the requirements
for the degree of Doctor of Philosophy

Abstract

the abstract

Contents

List of Figures

List of Tables

1

Introduction

1.1 Motivation

Six hundred thousand lower-limb amputees currently live in the United States according to recent estimates [Ziegler-Graham et al., 2008]. People undergo amputations due to a variety of reasons including traumatic injuries from workplace accidents, traffic collisions, and as casualties of war. In addition, a large percentage (54%) suffer from the loss of a limb due to complications arising from dysvascular disease associated with diabetes. Consequently, largely due to the expected increase in diabetes in the coming years, Ziegler-Graham et al. [2008] estimate that by 2050 the number of amputees living in the United States will likely double.

Currently, prosthetists often prescribe transfemoral amputees (those with amputations between the hip and knee joints) an energy storage and return composite foot such as the Sierra Foot (Freedom Innovations; Irvine, CA; fig. 1.1c) along with a microprocessor-controlled, mechanically-passive knee prosthesis. These knee prostheses feature control algorithms that measure kinematic and force data via sensors embedded in the device and adjust the knee's resistance accordingly. Examples of microprocessor-controlled prosthetic knees include the C-Leg (Otto Bock; Duderstadt, Germany; fig. 1.1a), which has an adjustable hydraulic damping system, and the Rheo Knee (Össur; Reykjavik, Iceland; fig. 1.1b), which achieves variable damping via a magnetorheological fluid. While Johansson et al. [2005] show these microprocessor-controlled knees can improve amputee gait characteristics by decreasing metabolic energy consumption and peak hip torque and increasing gait smoothness over that provided by fully-passive knee prosthesis, these prostheses still cannot fully replicate healthy leg behavior as they are incapable of providing positive power during the gait cycle.

Positive power at the knee is evident in a number of locomotion

(a) C-Leg™ Knee ©Ottobock

(b) Rheo™ Knee ©Össur

(c) Thrive™ Foot ©Freedom Innovations

Figure 1.1: Examples of microprocessor-controlled mechanically-passive knee prostheses (a,b) and a energy storage and return ankle-foot prosthesis (c).

tasks including level walking [Perry and Burnfield, 1992], walking up stairs [Nadeau et al., 2003], running [Buczek and Cavanagh, 1990], and jumping [Hubley and Wells, 1983]. In addition, active knee flexion and extension muscle activations have been noted during stumble recovery [Eng et al., 1994]. At the ankle joint, passive spring-like prostheses cannot replicate the positive net work seen in the ankle joint during level ground walking, which is essential for push-off and forward propulsion [Perry and Burnfield, 1992].

Consequently, lower-limb amputees, and especially transfemoral amputees[1] equipped with mechanically-passive prostheses suffer from a number of issues including markedly increased energy consumption [Waters et al., 1976], abnormal gait kinematics [Jaegers et al., 1995], and an increased likelihood of falling [Miller et al., 2001]. Specifically, large percentages of transfemoral amputees report they are unable to complete tasks such as walking outside in inclement weather (47.4%), walking while carrying a load (42.7%), walking up or down stairs without a handrail (38.5%, 37.9%), walking outside on uneven terrain (29.5%), picking up an object from the ground (28.1%) or getting up from the floor after a fall (22.8%) [Gauthier-Gagnon et al., 1999].

Importantly, these gait pathologies can lead an avoidance of walking [Gauthier-Gagnon et al., 1999]. This is especially true in the case of falls. Miller et al. [2001] find 49.2% of lower limb amputees feared falling and that of those afraid of falls 76% avoided physical activity as a result. Avoidance of physical activity is eminently concerning as it may lead to reduced strength, endurance, and balance, feeding a positive feedback loop that causes further debilitation.

To help remedy this situation, in the past decade researchers and companies have developed robotic powered knee and ankle prostheses for lower-limb amputees. These prostheses feature actuators at the knee and/or ankle that, if controlled correctly, could potentially

[1] those with above the knee amputations

Figure 1.2: Vanderbilt University's Robotic Transfemoral Prostheses.

(a) Generation 1   (b) Generation 2   (c) Generation 3
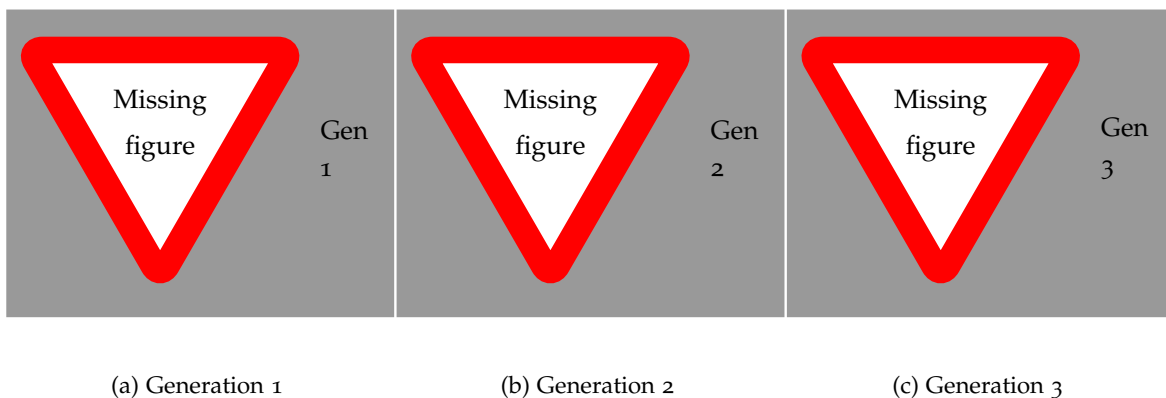
restore the kinetics, kinematics, and reactions of the healthy human leg. Notable examples include three generations of transfemoral prostheses developed by Vanderbilt University (fig. 1.2) [Sup et al., 2009, Lawson et al., 2013, 2014] and the Biom powered ankle (fig. 1.3) [Herr and Grabowski, 2011]. These powered prostheses have helped amputees walk on level ground more naturally and efficiently, as well as walk up stairs and slopes [Sup et al., 2011, Lawson et al., 2013], run [Huff et al., 2012, Shultz et al., 2015], perform sit-to-stand [Varol et al., 2009], and dance [Rouse et al., 2015]. These results illustrate the benefits of powered prostheses as many of these tasks require positive joint power and thus would be difficult to perform with mechanically-passive prostheses.

1.1.1   Challenges in Transfemoral Prosthesis Control

It still remains an open research question how best to control these prostheses to achieve natural and robust gaits. In the most established control method for powered prostheses, the prosthesis uses simple functions to approximate the joint torque versus angle relationship, termed the *quasi-stiffness* observed during walking [Sup et al., 2007, Lenzi et al., 2014b]. However, since the torque functions only approximate steady, level walking, this method requires further tuning to handle other situations such as walking on slopes [Sup et al., 2011] or rough ground [Thatte and Geyer, 2016] and changing foot placement targets [Schepelmann, 2016].

As mentioned earlier, walking on slopes and rough ground present major hurdles for transfemoral amputees. Moreover, previously developed prosthesis controls have not specifically addressed the risk of falling that is so detrimental to amputee quality of life. Therefore, it is clear that we should formulate a prosthesis controller with more power to generalize to a larger variety of environments, which will improve amputee gait robustness. Formulating a robotic prosthesis controller to accomplish this goal requires we address three main challenges:

Challenge 1: Human locomotion is a dynamic task During stance, the leg acts in a compliant, spring-like manner [Geyer et al., 2006] and significant time is spent in statically-unstable contact on the heel or toe, suggesting the importance of mechanical stability achieved via foot placement [Perry and Burnfield, 1992]. During swing, ballistic motion explains much of the leg trajectory [Mochon and McMahon, 1980]. Indeed, much of the entire gait cycle can be explained via passive dynamics as evidenced by passive-dynamic walkers (fig. 1.4) that can stably walk down slight inclines with no onboard power source [McGeer, 1990, Collins et al., 2005].

Figure 1.3: Biom Robotic Ankle Prosthesis
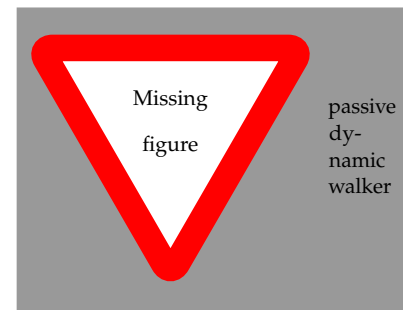
Figure 1.4: A passive dynamic walker walks down hill with no internal actuation highlighting the role of natural dynamics in walking.

Consequently, in order to ensure that amputee gaits are natural and efficient, but still robust, it is essential that robotic prosthesis controllers not only admit, but leverage the inherent dynamics of walking. Therefore, the required control paradigm cannot follow strategies often used for humanoid locomotion (for example on Honda's Asimo Robot fig. 1.5) that employ position control in order to track preplanned, statically-stable gaits. Rather, the control strategy should interact dynamically with the amputee by governing interaction forces instead of mandating kinematic objectives.

Challenge 2: We have incomplete state information An additional difference between robotic prosthesis control and controls often used on humanoid walking robots stems from the lack of full state information. Humanoid walking controllers such as those used in the DARPA robotics challenge (DRC), controllers use the full state of the robot (*i.e.* the positions and velocities of every joint and the robot's center of mass), to plan and track a trajectories, thereby ensuring stability of the full system [Feng et al., 2015, Kuindersma et al., 2014, Englsberger et al., 2014].

While these recent approaches used in the DRC are dynamic and therefore address challenge 1, for prosthesis control we typically only know the state of the prosthesis itself. It is unreasonable to expect that amputees will don full body sensing suits in order to provide a complete picture of the state of the amputee-prosthesis system. Therefore, prosthesis controllers must be decentralized, meaning joint torque commands are computed using only a subset of the full state. A side affect of this approach is a loss of formal stability guarantees. However, we can still evaluate amputee stability empirically.

Challenge 3: Amputees are unique Finally, we should be able to adapt robotic prosthesis controllers to each amputee's individual needs. The variation in amputee needs arise from a number of factors including, but not limited to, the amputee's height, weight, strength, endurance, reason for amputation, time since amputation, experience, and personal preferences. Consequently, prostheses and controllers should be optimized to suit individual users.

This thesis proposes dynamic decentralized control methods for transfemoral prostheses, along with methods to optimize them for individual amputees, in order to improve gait robustness and naturalness.

1.1.2   *Approach*

In this thesis, we seek to improve amputee gait robustness and naturalness by employing an alternative approach to joint control in
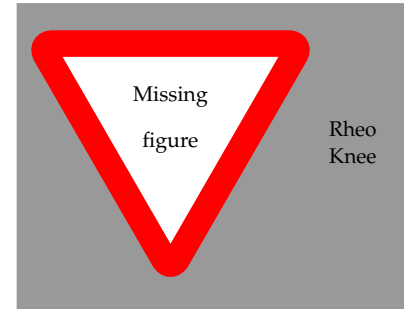
Figure 1.5: Honda's Asimo Robot uses position control and statically stable gaits.

prostheses that seeks to mimic the underlying dynamics and control of the human neuromuscular system. In this approach, instead of replicating recorded torque profiles with quasi-stiffness functions, we model the dynamical system, consisting of virtual muscles and local reflex feedback pathways, that generate joint torques during locomotion. Crucially, the resulting prosthesis control addresses challenges 1 and 2: the control is decentralized, as the reflex feedback are designed to rely only on the state of other muscles in the same leg, and dynamic, as the virtual muscles integrate the sensed kinematic state of the prosthesis in order to generate desired torques, not positions, at the joints. These torques, along with the reaction forces in the amputee's socket and on the ground shape the motion of the amputee-prosthesis system.

Prior work on neuromuscular models shows that when applied to simulated biped models they can produce robust gaits with natural appearances. For example, using a neuromuscular model, an optimized simulated biped model walked on unseen, uneven terrain with sudden drops and steps up to 14 centimeters [Song and Geyer, 2015]. In addition, Eilenberg et al. [2010] successfully applied the neuromuscular control approach to a powered ankle prosthesis (fig. 1.6), which mimics the kinematics and kinetics of the ankle joint in human walking including its adaptation to sloped environments. It remains unclear, however, whether we can extend the approach to transfemoral prostheses with both knee and ankle joints.

Therefore, to motivate our specific choice of neuromuscular control for improving amputee gait stability, in completed work, we construct a simulation of the amputee-prosthesis system and compare the gait robustness achieved by neuromuscular control versus the established impedance control method. We find that neuromuscular control enabled the simulated amputee to walk further over rougher terrain than the established impedance control method allows.

Next, to test the feasibility of the control approach to control a real system, we design and build a partial powered transfemoral prosthesis prototype with an active knee actuator and a passive, spring-loaded ankle. The prosthesis prototype uses series elastic actuation [Pratt and Williamson, 1995] that allows it to accurately achieve the torques commanded by the neuromuscular model. Initial tests with an intact user wearing the prosthesis through an amputee simulator adaptor show that the proposed neuromuscular control, when applied to the knee of an active prosthesis, produce reasonable kinematics and joint torques. This positive result motivates continued development of the prosthesis into a full active knee and ankle transfemoral prosthesis and implementation of testing of the full neuromuscular prosthesis control.
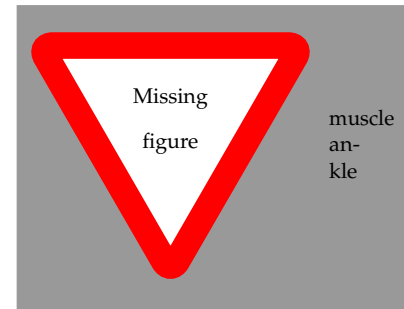
Figure 1.6: Eilenberg et al. [2010] simulate virtual muscles in order to control an ankle prosthesis.

To address the challenge 3, we propose to optimize prosthesis controls for specific subjects. To this end, in completed work, we develop an algorithm that uses preference feedback from users to optimize control system parameters. We test the method on problems of increasing relevance: first by optimizing synthetic reward functions, then optimizing the parameters of simulated dynamical systems, and finally by optimizing neuromuscular control parameters for intact users wearing the prosthesis through an amputee emulator brace. The results suggest the proposed optimization method outperforms baseline methods for optimizing from user preferences. However, it remains to be seen if the proposed method improves gait characteristics when applied to the full neuromuscular controlled prosthesis for an amputee subject. We intend to investigate this question via additional tests on an amputee subject.

Last, we seek to improve the capability of the transfemoral prosthesis to respond to trips, which pose a significant and impactful threat to amputee quality of life. To accomplish this goal, we propose to use imitation learning techniques [Argall et al., 2009] to learn polices that allow the prosthesis to appropriately respond to disturbances during swing. The proposed method to learn these policies will address challenges 1-3 in that it will be a decentralized control that only uses information from the prosthesis and be dynamic and personalized by working with each amputee' innate trip response reflexes.

Previous work in this area has trained classifiers on data obtained by tripping healthy human subjects [Lawson et al., 2010, Shirota et al., 2014]. The authors then evaluate these classifiers via cross validation, in which a subset of the training data is set aside and used for testing, and report low error-rates. However, to date no one has applied a trip classifier to prosthesis hardware in order to initiate a trip recovery controller. Trivial application of classifiers trained on healthy human subject data likely will yield poor results, as the distribution of data at test time generated by a prosthesis that is controlled by a learned policy will differ from the data used to train that policy. The training and test time distribution mismatch violates the i.i.d.[2] assumption that underpins classification performance. To remedy this problem, we intend to employ the DAGGER training method [Ross et al., 2011] that aligns the train and test time distributions through an iterative procedure. We will collect training and testing data to learn and evaluate the trip recovery policies using the Push Bot robot (fig. 1.7) which can apply tripping forces to subjects via actuated tethers.
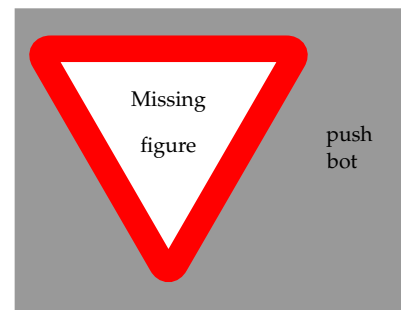
Figure 1.7: Push Bot robot for training and evaluating trip recovery policies

[2] independent and identically drawn

1.2 Expected Contributions

Work presented in this thesis will advance the state-of-the-art for robotic transfemoral prosthesis control and optimization. There are four main expected contributions:

Contribution 1: A series elastic prosthesis design We present the design of a transfemoral prosthesis featuring series elastic actuators (SEAs) capable of accurately producing the torques commanded by the neuromuscular model, generating enough torque and speed to enable trip recovery experiments, and handling the impact loads expected during trip recovery experiments. We have made significant progress towards this contribution already by completing the design, manufacturing, assembly, and initial testing of the prosthesis' knee joint as well as the design and fabrication of its ankle joint. Figure 1.8 shows the current stage of the prosthesis prototype with the completed SEA knee and a passive spring-loaded ankle well as a CAD render of the expected completed prosthesis design.

Contribution 2: A method for optimizing systems via preferences We present a new algorithm for optimizing systems, such as prostheses, using user preferences. The algorithm uses preferences between pairs of control parameters to circumvent having to define or learn an explicit reward function for each user. Additionally, the algorithm employs Bayesian optimization techniques in order to query users for preferences that are expected to maximally reduce the uncertainty of the location of the optimum parameters.

Contribution 3: Evaluation of neuromuscular transfemoral prosthesis control We will implement the proposed neuromuscular prosthesis control on the SEA transfemoral prosthesis, optimize its parameters according to the amputee subject's preferences, and evaluate the prosthesis' ability to produce a natural and robust gait. We will measure gait characteristics in terms of joint kinematics and kinetics and the amputee's metabolic energy consumption. We will present results relative to typical non-amputee gait, the amputee's gait using his or her prescribed prosthesis, and the gait achieved by an unoptimized prosthesis control. We will also evaluate the ability the control to adapt to novel circumstances such as changes in gait speed and ground slope.

Contribution 4: Learning and evaluation of trip recovery policies The last contribution is a method to learn and evaluation of trip response policies for recovering from disturbances during swing. The learned policies will advance the state-of-the-art as they will be the first trip recovery policies implemented on real prosthesis
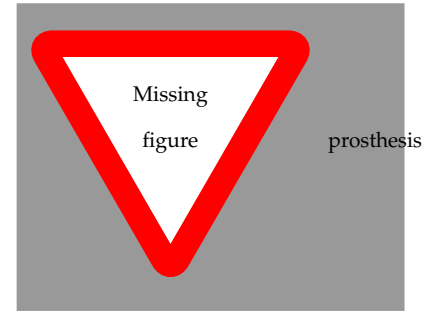
Figure 1.8: Proposed SEA prosthesis design

hardware, whereas previous policies were trained and tested offline using data collected from non-amputee subjects.

2

Background

The main goal of this thesis is to improve transfemoral amputee gait robustness and naturalness by applying neuromuscular models of human locomotion to control prosthesis hardware capable of dynamic locomotion. Existing approaches to walking control in humanoid robots and prostheses have largely failed to reach the levels of stability and dynamism required to match that of an amputee's lost limb. In this chapter, we will review these existing approaches, examine their strengths and weaknesses, and motivate our specific control and design choices.

Section 2.1 categorizes approaches to walking control into four major groups based on their ability to produce dynamic interactions with the environment (dynamic vs kinematic) and whether they can produce control commands using only a subset of state (decentralized vs centralized). As mentioned earlier, only dynamic, decentralized controls address challenges 1 and 2 of amputee locomotion (section 1.1.1) and are thus suitable for prosthesis control. Section 2.2 dives deeper into a subset of dynamic decentralized control: bioinspired approaches that seek to model the function of the lost limb and are thus particularly well suited for prosthesis control. Section 2.3 reviews existing mechanical designs of active prostheses and examines their ability to enable dynamic locomotion. Finally, section 2.4 will discuss previous work towards empowering prostheses with active trip recovery modes via explicit detection and classification of stumbles.

2.1   *Fundamental Walking Dynamics and Control*

Simple point-mass models of walking can help us understand the fundamental dynamics that control must shape in order to achieve stable locomotion gaits. The simplest model that reproduces the center of mass trajectory and ground reaction forces seen during

human walking is the bipedal spring mass model [Geyer et al., 2006]. This model, illustrated in fig. 2.1, simplifies locomotion to a pair of compliant unidirectional springs connected to a point mass. When initialized with human-like mass and leg length, the model can generate characteristic features of human locomotion such as sinusoidal center of mass trajectories, M-shaped vertical ground reaction forces, S-shaped horizontal ground reaction forces, and the proper sequence of double and single support.

We will look at two paradigms for walking control: centralized approaches that use full state information and decentralized approaches that use a subset of state information. Centralized approaches typically utilize a model of the full system in order to compute control commands that project the full system's dynamics onto those of the simplified model. Usually, centralized approaches also place additional constraints on the center of mass (COM) dynamics in order to facilitate planning and ensure stability. In contrast, decentralized approaches typically do not explicitly model either the full system or the fundamental dynamics. Rather, these approaches use heuristics to generate motions and forces similar to those of the fundamental model.

2.1.1   Centralized Control

Kinematic centralized control is one of the oldest forms of locomotion control. The predominant approach in this category is based on the linear inverted pendulum model (LIPM) [Kajita and Tani, 1991, Kajita et al., 2001]. This simplified locomotion model applies additional reductions to the bipedal spring-mass model, replacing spring legs with ideal prismatic force sources and constraining the center of mass to move on a plane. The resulting simplified model features linear COM dynamics with respect to the zero moment point (ZMP). The ZMP is the point on the ground about the horizontal moments needed to counteract the total reaction forces on the system is zero. When the ZMP lies within the support polygon[1] (SP), it is coincident with the center of pressure (COP). On the other hand, if the ZMP moves beyond the SP, the system will begin to tip over the edge of the SP. In one dimension, the location of the ZMP is given by,

$$x_{ZMP} = x_{COM} - \frac{z_{COM}\ddot{x}_{COM}}{g}. \tag{2.1}$$

This equation relates the horizontal COM, x_{COM}, dynamics to the location of the ZMP, x_{ZMP}, given the height of the COM, z_{COM}, and gravitational acceleration g.

Based on this insight, researchers have developed numerous ZMP-trajectory methods that follow 5 basic steps:
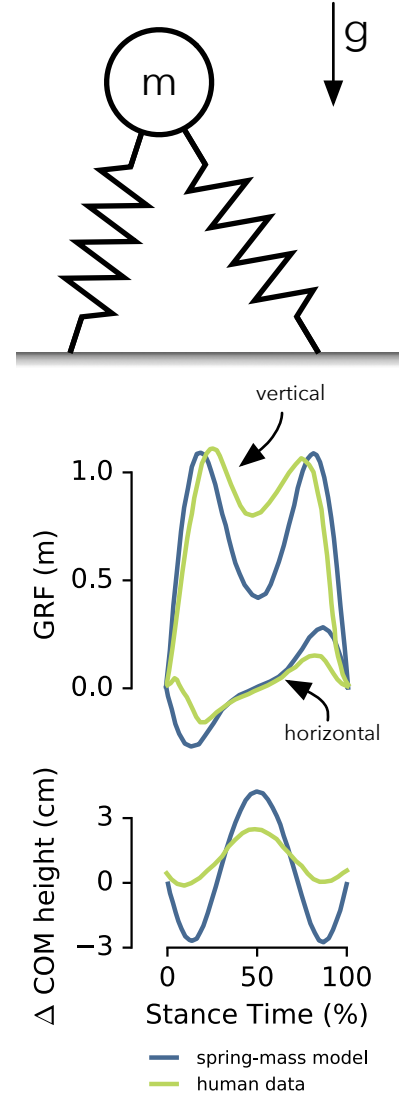
Figure 2.1: The bipedal spring mass model captures many fundamental features of human walking such as the M-shaped vertical ground reaction profile, S-shaped horizontal ground reaction profile and sinusoidal center of mass trajectory. Figure adapted from Geyer et al. [2006].

[1] The convex hull of contact points on the ground

1. Plan a series of foot steps given the terrain and task such that the induced sequence of support polygons contains no gaps.

2. Generate a ZMP trajectory that lies within the support polygons. Typically, it is desirable that the trajectory maintains its distance from the edges of the support polygons in order to provide a margin of stability.

3. Solve for the COM trajectory given the desired ZMP trajectory. This step requires inverting the solution to a differential equation, eq. (2.1), to solve for x_{COM}. Researchers have proposed numerous solutions to this problem including preview control [Kajita et al., 2003], and differential dynamic programming [Feng et al., 2015], the latter of which can solve for the ZMP and COM trajectories simultaneously.

4. Use inverse kinematics to calculate joint velocities that track the COM trajectory.

5. Track the desired joint velocities with servo controls.

A large number of robots have successfully employed this general framework to walk [Hirai et al., 1998], traverse uneven ground [Shimmyo et al., 2010], and run [Kajita et al., 2007]. Moreover, the method guarantees that for the nominal gait, the COP will remain in the SP, and thus the system will maintain its stability.

However, there are several key issues to this approach. One issue stems from steps 4 and 5 listed above. These steps generate and precisely follow via servo control a kinematic trajectory of joint angles. When perturbed by unforeseen external forces, stiff position control in this manner may generate large reaction forces and thus may move the COP outside of the SP, resulting in a fall. We can understand the interactions between the leg and the environment and the leg and robot body through the concepts of impedance and admittance. The environment and robot body are admittances, objects that take forces as inputs and move (or not move) in response. As discussed in Hogan [1985], it is therefore necessary that the leg acts like an impedance, an object that produces an interaction force in response to the position imposed on it by the environment and robot body.

Dynamic centralized control seeks to control these interaction forces by directly computing joint torques, instead of using high-gain position control. Commonly, in this approach the dynamics model of the full system[2],

$$M(q)\ddot{q} + C(q,\dot{q})\dot{q} + N(q) = S\tau + J^T(q)\lambda, \qquad (2.2)$$

[2] Where q, $\dot{q}$, and $\ddot{q}$ describe the generalized coordinates, velocities, and accelerations of the system configuration, $M(q)$ is the mass matrix, $C(q,\dot{q})$ is a matrix of centripetal and Coriolis force coefficients, $N(q)$ represents the gravitational forces, S is a selection matrix that assigns joint torques τ to coordinates q, $J(q)$ is the Jacobian between joint angles and contact points, and λ is a vector of external forces

is used as an equality constraint in a *quadratic program* (QP) that minimizes torques, reaction forces, and deviation from the desired trajectory. Additionally, the QP can include inequality constraints representing torque saturations and friction limits [Hutter et al., 2013, Herzog et al., 2014, Saab et al., 2013, Wensing and Orin, 2013]. Recently, at the DARPA Robotics Challenge (DRC) several robots used QP-based dynamic centralized approaches to control humanoid robots through a disaster relief scenario [Feng et al., 2015, Kuindersma et al., 2014, Englsberger et al., 2014].

While the replacing steps 4 and 5 with a QP-based torque control can help improve dynamism and compliance, the resulting biped gaits of these strategies do not resemble human gaits for two reasons: First, the linear inverted pendulum model does not produce center of mass trajectories or ground reaction force profiles similar to those seen during human locomotion. Second, human gaits do not constrain the ZMP to the support polygon as we spend significant time on the heel and balls of our feet during stance [Perry and Burnfield, 1992].

To overcome these issues and produce more human like gaits, recently researchers have investigated applying dynamic centralized control approaches to enforce spring-mass model dynamics instead of LIPM dynamics. With this approach, researchers have developed robust controllers for both walking [Wensing and Orin, 2013] and running [Martin et al., 2015] for humanoid robots. Alternatively, Sreenath et al. [2011] replaced the LIPM model with a one-degree-of-freedom walking mechanical linkage. In this control, all joint angles are parameterized with respect to a single phase variable, usually the leg angle. As the phase variable progresses via its passive dynamics a control Lyapunov function impose virtual constraints that force joints to follow a walking gait trajectory. The control expresses a degree of dynamism, as the phase variable is free to evolve naturally, and demonstrates human-like reflexes as it is automatically maintains its balance in response to external perturbations by stepping forward or backwards.

While centralized control approaches have helped close the gap in dynamism and reactiveness displayed by humans and robotic systems, these methods can also suffer from their reliance on an accurate model of the system dynamics (eq. (2.2)). It may be difficult to identify the parameters of this model, such as friction and damping coefficients and inertias, especially for prosthesis systems. Consequently, researchers have explored decentralized control methods that use only a subset of the state and generally rely on heuristic control strategies instead of deriving control actions from a detailed system model.

2.1.2 *Decentralized Controllers*

In contrast to the centralized control methods discussed in the previous section, decentralized methods generate walking gaits without requiring measurement of the full system state. Consequently, decentralized walking strategies typically do not involve planning[3] and do not enjoy stability guarantees. Rather, gait emerges naturally from the coupled dynamics of several closed-loop systems. In the case of prosthesis control, one system is the human neuromuscular system and the other is the closed-loop dynamics of the robotic prosthesis.

[3] steps 1 to 3 of the centralized control framework

For example, the earliest robotic prosthesis control strategy, termed *echo control,* records the kinematics of the healthy leg and then executes an identical trajectory on the prosthesis on the following step [Grimes et al., 1977, Grimes, 1979]. This strategy, as with all robotic prosthesis controls we will review, does not require measurement of the torso, head, or arm movement. Also, during execution of the trajectory, the position servo controls only require measurement of the prosthesis joint angles, making it more practical for implementation on a prosthesis device. However, this control is an example of a *kinematic decentralized control.* Consequently, it suffers from many of the same problems identified in centralized kinematic control. Namely, it does not comply to the environment, which can result in large and unnatural reaction forces. For example, if a prosthesis under this control strategy encountered an obstacle during swing, the knee would not to flex in response, thereby inducing a large moment on the amputee. Moreover, echo control suffers from the problem of not allowing the amputee to to start or stop gait with their prosthesis leg.

As was the case for centralized control, commanding torques instead of joint angles helps alleviate this issue by allowing for compliant interaction with the environment. *Dynamic decentralized control* typically features a finite state machine with states representing different phases of gait such as stance and swing. Within each phase, a heuristic control law specifies the torque command. For example, the first robotic system to achieve stable, dynamic locomotion employed simple heuristics to regulate the height, velocity, and attitude of 2 dimensional one legged hopping robot [Raibert et al., 1983]. Specifically, to control the height of the robot, the control adjusts the duration of thrust generated by the prismatic leg actuator during stance. Researchers empirically determined the relationship mapping thrust duration to hopping apex height. To control horizontal velocity, first it is assumed that placing the foot in the center of the locus of points comprised of the center of gravity projected onto the floor will result in zero change in horizontal velocity. Then, a linear

feedback gain on velocity error determines the offset from this point. A servo control on the leg angle during swing realizes the desired foot placement. Finally, the control regulates the torso attitude during stance via PD feedback.

Unlike a centralized control scheme, Raibert et al.'s scheme does not consider the interaction between these control modules, preferring instead to treat stabilization of each degree of freedom as an independent task. Regardless, the system demonstrated remarkable dynamism and robustness, allowing the hopping robot to jump 0.25 m, run 1.2 m/s, and recover from horizontal disturbance forces applied by an experimenter. Moreover, the control strategy easily extended to 3D locomotion as well without an exponential increase in computation complexity. This seminal work demonstrates that LIPM-based, centralized control that carries stability guarantees is not necessary to ensure stability of robotic systems and suggests the constraints and model reductions enforced by centralized control may hold systems back. Rather, intelligent design of heuristic control to shape the natural dynamics of a system can in fact provide high levels of performance in practice.

Virtual model control, proposed by Pratt et al. [2001], provides a convenient method for designing heuristic control strategies. In contrast to the control proposed in Raibert et al. [1983], which commands forces aligned with the robot's actuators, virtual model control does not require such correspondence. Rather, designers can use their intuition to place virtual mechanical elements, such as springs, dampers, masses, and linkages on or between reference coordinate frames located anywhere in space. The virtual mechanisms apply generalized forces F to the coordinate frames, which are translated to joint torques τ via the Jacobian J according to

$$\tau = J^T F. \tag{2.3}$$

Joint-level controls realize these desired torques, thereby simulating the virtual components.

This control approach has many advantages: First, it provides an intuitive framework to design controllers for many tasks and many different robot architectures. Second, even though the original virtual model control proposed by Pratt et al. is centralized, one can easily design decentralized controllers with this method as well. If the virtual mechanisms do not span all the joints, J will be a sparse matrix, resulting in a decentralized control approach that can be applied to prostheses. Last, impedance mechanisms such as springs and dampers ensure dynamic interaction with the environment with reasonable reaction forces.

2.1.3   *Dynamic Prosthesis Control*

With the goal of dynamic interaction with the environment in mind, Sup et al. [2007] formulated *impedance control* for active prostheses. The strategy is a essentially a form of simple virtual model control, where linear and nonlinear springs along with linear dampers span individual joints. A finite state machine, such as the one in fig. 2.2, switches impedance functions as the amputee progresses through phases of gait: early and late stance and early and late swing. The impedance functions in this strategy actually describe the *quasi-stiffness* of the joint [Rouse et al., 2013], which is the torque vs angle curve seen during walking. Therefore, we will henceforth, refer to this strategy as quasi-stiffness control for prostheses.

To describe the quasi-stiffness curve, Sup et al. [2008] uses a piece-wise model with linear and cubic stiffness terms, and a linear damping term.

$$\tau = -k_1(\theta - \theta_0) - k_2(\theta - \theta_0)^3 - b\dot{\theta}. \tag{2.4}$$

Regression analysis of the torque versus angle and velocity data of intact subjects performing level-ground walking returns the quasi-stiffness parameters for each joint in each state. An experimenter can further tune these parameters to better suit the amputee's gait.

This strategy has been implemented on both transtibial [Shultz et al., 2014] and transfemoral [Lawson et al., 2014] active prostheses and has improved amputee gait characteristics over those provided by passive prostheses. Moreover, by tuning impedance parameters for specific tasks and augmenting the finite state machine, researchers have extended impedance control to help amputees to walk up and down slopes [Sup et al., 2011] and stairs [Lawson et al., 2013], run [Huff et al., 2012, Shultz et al., 2015], and execute sit-to-stand motions [Varol et al., 2009]. Lenzi et al. [2014b] present a similar method, in which a look-up-table directly stores the quasi-stiffness curve with respect to angle and velocity. With this method, Lenzi et al. obtain speed adaptation by linearly interpolating between two look up tables representing slow and fast walking.

In contrast to the kinematic echo control strategy discussed earlier, quasi-stiffness control should produce more reasonable interaction forces. This is especially true when the prosthesis encounters an unexpected disturbance, as the control does not try to follow a specific trajectory with high precision and thus high feedback gains. However, whereas impedance control as originally proposed by Hogan [1985] advocated independent specification of the disturbance response torque and the torque required to achieve the desired motion, the quasi-stiffness control strategies we have discussed use the same behavior for both.
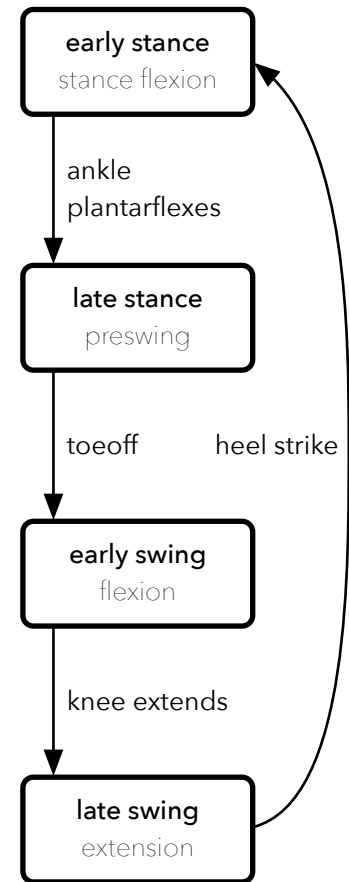
Figure 2.2: Finite state machine used for the quasi-stiffness control proposed by Sup et al. [2007]. In each state the control employs impedance functions that determine the behavior of the ankle and knee joints of an active transfemoral prosthesis.

Recently, several research efforts have investigated dynamic control strategies that provide both a feed forward element that generates the desired motion and a feedback element that responds to disturbances. Such approaches allow one to tune these these two aspects separately. While these approaches are decentralized in that they do not require state information of the amputee, they do borrow aspects of centralized approaches such as trajectory planning, and model-based computation of feed-forward torques.

For example, Lenzi et al. [2014b,a] compute minimum jerk trajectories for the knee and ankle joints during the swing phase. These trajectories are parameterized by fifth order polynomials that connect the initial states of the knee and ankle joints, measured just before toe-off, to to the desired final states, specified for both joints as zero angle, velocity, and acceleration. The ankle joint uses a single trajectory, while the knee joint uses two trajectories, one that connects the initial state to a maximum knee flexion state and one that connects the maximum knee flexion state to the final state. Using a model of the system represented by Euler-Lagrange dynamics equations (eq. (2.2)) one can calculate the required feed forward torque to follow the planned trajectories. Minimizing the jerk, the derivative of acceleration, helps ensure smoothness of the computed torques. A proportional derivative feedback control then determines the disturbance response behavior. The use of a strong feed forward term allows for lower PD feedback gains and more compliant behavior.

A disadvantage of the minimum jerk trajectory approach is it generates and executes a trajectory whose duration is heuristically determined at toe-off. Recently, Gregg et al. [2014], Zhao et al. [2016] have proposed methods similar to the centralized virtual constraint control discussed in section 2.1.1, in which the natural progression of a phase variable determines the rate at which the control follows preplanned trajectories. Gregg et al. [2014] chooses to follow the ankle-foot and knee-ankle-foot rollover shapes, which are defined as the location of the center of pressure with respect to coordinate systems attached to the shank and the ankle-hip line respectively. The center-of-pressure naturally becomes the phase variable for these trajectories. The observation that the roll-over shapes are invariant across walking speed, shoe geometry, and amputee weight motivates this choice. In this strategy, a model-based feedback linearization controller enforces adherence to these desired trajectories as the center of pressure progress through its natural dynamics. This formulation provides both the feed forward torque command and a disturbance response command that provides exponential converge to the desired rollover shapes.

As we noted earlier for centralized robotic control approaches,

a downside of these two trajectory following controllers is their reliance on accurate dynamics models to compute feed forward torques. To overcome this issue, Zhao et al. [2016] propose a model-independent virtual constraint control. In this scheme, quasi-stiffness control provides a feed-forward torque signal that reduces the dependence on the model. A quadratic program then computes the minimum required extra effort to ensure convergence to a preplanned trajectory that is parameterized with respect to hip angle.

2.2 Bioinspired Control for Prostheses

The dynamic control prosthesis control strategies we outlined in the previous section in some sense all provide a feed-forward torque that generates a desired nominal trajectory, and an impedance behavior that determines the disturbance response characteristics. In the case of quasi-stiffness control, the same function encodes both of these characteristics. In the case of trajectory following controllers, model inversion provides the necessary torque to execute the plan while either a proportional derivative controller, feedback linearization, or control Lyapunov function provides impedance behavior. However, it is not clear that these approaches generate the impedance responses of the system we actually want to replicate in the field of prosthetics, that of the amputee's missing limb. In the biological leg, impedance characteristics may play a crucial role when it comes to stabilizing movement [Won and Hogan, 1995, Burdet et al., 2001] and changes in response to a number of factors including any of mean ankle torque, ankle position, perturbation amplitude, and muscle fatigue [Kearney and Hunter, 1989].

An alternative approach to developing prosthesis control, which may better model joint quasi-stiffness and joint impedance, is to model the underlying biological neuromuscular dynamical system that gives rise to these characteristics. Two hypothesized mechanisms that govern the neuromuscular system are central pattern generators (section 2.2.1) and reflexes (section 2.2.2). These two mechanisms are naturally decentralized and dynamic and are thus attractive models to utilize in a prosthesis controller.

2.2.1 Central Pattern Generators

Central Pattern Generators in Biology

Central Pattern Generators (CPGs) are hypothesized nonlinear oscillators, comprised of neurons in the central nervous system, that can autonomously generate periodic neural activation patterns [Ijspeert, 2008]. Brown [1911] first suggested their existence based on experi-

ments he conducted on decerebrated and deafferented cats. In these experiments, Brown severed both the *afferent pathways* (that carry sensory information) and *efferent pathways* (that transmit higher level commands from the brain to motor neurons). Despite the lack of high level control and sensory feedback, the cats still displayed cyclical motions in their hind legs similar to those seen during normal gait. This result suggests CPGs may play an important role in generating locomotion controls in vertebrate animals. Similar cyclical neural activity (called fictive locomotion) has been found in isolated lamprey spinal cords [Cohen and Wallén, 1980], salamanders [Delvolvé et al., 1999], and frog embryos [Soffe and Roberts, 1982].

Moreover, research has shown that stimulation of a region of the brain stem called the Mesencephalic Locomotor Region (MLR) can manipulate the neural activity generated by CPGs. For example, electrical stimulation of the MLR led to gait transitions in both decerebrated cats [Shik et al., 1966] and salamanders [Cabelguen et al., 2003]. Therefore, CPGs may serve as a form of dimensionality reduction and decentralization for the biological control system as low-dimensional, high-level signals from brain can shape the high-dimensional, low-level CPG output. Consequently, CPGs may also represent an attractive option for robotic legged locomotion controllers as decentralization and dimensionality reduction are desirable properties in this domain as well.

Neuromechanical Models with CPGs

The seminal work on CPG-based bipedal locomotion control is presented in Taga et al. [1991]. In this model, a CPG neural network of six interconnected oscillators describes the joint torques applied to a four link biped model. Differential equations, first presented in Matsuoka [1987] with additional sensory feedback from joint and inertial link angles, describe the output of the CPG network. The resulting biped model walks with a natural gait featuring both single and double support and demonstrates robustness to a variety of disturbances including changes to ground stiffness, damping, and slope. Additionally, tuning a single parameter induced a transition from walking to running in the model in a manner comparable to the biological gait transitions observed after stimulation of the MLR.

CPGs have successfully controlled several bipedal humanoid robots. For example, Endo et al. [2005] used Matsuoka's nonlinear oscillators along with by bio-inspired feedback pathways that regulate ground reaction forces and body roll to generate desired foot trajectories for the bipedal QRIO robot. As in Taga et al.'s simulations walking speed can be controlled via adjustment of a single parameter
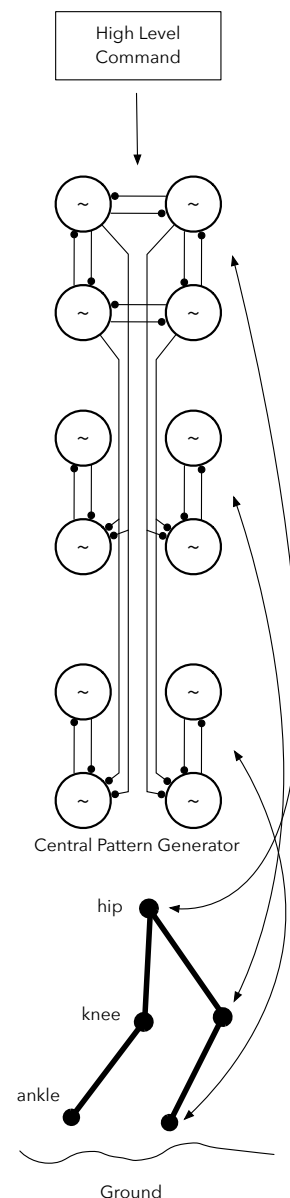
Figure 2.3: Central Pattern Generator for bipedal locomotion as described in Taga et al. [1991]. Six neural oscillators receive feedback from and command joint torques for the hips, knees, and ankles of a planar biped model. A one dimensional high-level control signal enables control of speed and elicits gait transitions.

and the robot is robust to changes in step height. Authors have also successfully employed other nonlinear oscillator models. In Shan and Nagashima [2002], a Recurrent Neural Network generates oscillatory signals for a 20-DOF humanoid robot, HOAP-1, that allow it to walk up and down stairs. In Righetti and Ijspeert [2006], programmable "Hopf" oscillators [Righetti et al., 2006] learn desired walking trajectories through entrainment enabling HOAP-2, a 25-DOF robot, to walk forwards and backwards at varying speeds and step lengths.

CPGs for Prosthesis Control

CPGs have also been proposed for controlling both mechanically-passive and active lower limb prostheses. Nandi et al. [2009] optimize CPG parameters to fit recorded knee angle trajectories from healthy human subjects. During walking, the CPG entrains desired knee motions to the oscillations of the amputee's hip joint. The desired knee angles are achieved in a mechanically-passive prosthesis via online adjustment of the knee damping. Similarly, Torrealba et al. [2010], Mora et al. [2012] also use a CPG to control a mechanically-passive variable damping prosthesis but use phase resetting to synchronize the amputee and CPG dynamics.

For active prostheses, Geng et al. [2012] suggest using a Hopf oscillators to fit the trajectory of the knee angle during walking. Guo et al. [2010] extend the idea of using a CPG for active prosthesis control by proposing a hierarchical approach with a support vector machine (SVM) at the high-level inferring amputee intent from EMG signals, and a CPG at the lower-level determining the desired knee and ankle angles for an active transfemoral prosthesis. However, in both cases, the authors do not provide experimental results on real prosthesis hardware. Moreover, unlike in Taga et al.'s original work, these proposed CPG networks for prostheses generate desired joint kinematics instead of torques. Consequently, these controllers may not allow prostheses to exhibit the dynamism and compliance we desire.

2.2.2   *Neuromuscular Reflexes*

Neuromuscular Reflexes in biology

Around the same time Brown hypothesized the existence of central pattern generators, Sherrington [1910a,b] suggested another mechanism for oscillatory neural signals: chains of *reflexes*, or local feedback loops, that trigger in response and entrain to sensory signals. Sherrington identified complex, multi-joint, multi-limb reflex arcs involving both excitation and inhibition in response to cutaneous

stimulation in decerebrated cats. Moreover, he observed rhythmic stepping behavior in decerebrated cats suspended off the ground and concluded that the behavior emerged reflexively based on proprioceptive signals emanating from the muscles themselves and not from centrally generated oscillatory signals.

In animal experiments discussed earlier, while CPGs can go a long way towards explaining locomotion neural activity, they still do not fully explain all observed phenomena. Reflexes likely at least shape locomotion activation patterns through entrainment, for example in Lamprey's movement of the tail generates activation in the spinal chord of equal frequency [McClellan and Jang, 1993], and phase resetting, as demonstrated by the ability of decerebrated cats to walk on treadmills across a range of speeds [Rossignol, 2000].

For human and primate bipedal locomotion, the role of CPGs is more muddied and the role of reflexes more evident than for decerebrated cats and simpler vertebrate animals [MacKay-Lyons, 2002, Vaughan, 2003, Nielsen, 2003]. This is perhaps due to the demands of controlling the inherently unstable dynamics of upright walking [Capaday, 2002]. For example, while rhythmic spinal activity has been observed in humans, it is not clear if the neural signals are an example of autonomous fictive motion, indicative of a CPG, or entrainment with stretch reflexes in leg muscles [Capaday, 2002, Stewart et al., 1991]. In this case, we can also look to robotics to provide insight about biology: in the previously discussed experiments on humanoid robots controlled by CPGs, a significant reduction in robustness was observed after blocking sensory feedback pathways [Endo et al., 2005, Righetti and Ijspeert, 2006] indicating CPGs alone may not fully explain bipedal locomotion. Whereas research has not yet clearly established the presence of a CPG driving human locomotion, research has identified many reflexes that contribute to locomotion such as the Hoffman reflex (H-reflex) of the soleus ankle plantarflexor muscle [Capaday and Stein, 1987], stretch reflex in the soleus [Yang et al., 1991], soleus force feedback [Grey et al., 2007], and cutaneous reflexes that induce withdrawal responses [Yang and Stein, 1990].

Neuromuscular Models with Reflexes

To model the potential interplay between muscular reflexes and CPGs in human locomotion Ogihara and Yamazaki [2001] extend the model presented in Taga et al. [1991] by adding muscles stimulated by alpha motor neurons. This model simulates nine muscles of the leg, each stimulated by an alpha motor neuron that receives input from a CPG oscillator and proprioceptive feedback from one or more muscles. The muscles produce forces according to their state and

activation input (computed using models presented in Pierrynowski and Morrison [1985] and Davy and Audu [1987]). These forces are applied to constant moment arms in order to produce joint torques summed about joints as in a virtual model control. The authors optimize the cost of transport of transport of the biped with a genetic algorithm and achieve a gait with human-like kinematics and kinetics. Moreover, the forces produced by many of the muscles resemble those produced during human locomotion. Despite the fact that the CPG used in this model received no feedback signals, the resultant gait still exhibited a small degree of robustness to perturbations although not as much as Taga et al.'s model. The author's attribute the robustness to the stabilizing feedback provided by muscle reflexes.

Whereas models and robot experiments show reflexes are vital for maintaining bipedal gait stability, the same cannot be said about CPGs. In fact, as shown by Geyer and Herr [2010], it is possible to simulate robust and human-like bipedal locomotion using only reflexes. This work employs a neuromuscular model, similar to that used in Ogihara and Yamazaki [2001], but does away with the feed forward CPG stimulations sent to alpha motor neurons. Instead, Geyer and Herr hypothesize the existence of several force and length muscle reflexes that implement three key aspects of bipedal locomotion: compliant leg behavior, preventing joint over extension, and providing trunk stabilization. The gait achieved by this model is more robust than and more accurately reproduces kinematics, kinetics, and ground reaction forces seen in human walking than Ogihara and Yamazaki's model. Moreover, it also produces human-like stimulations for many of its muscles.

While we cannot say based on this result alone that CPGs do not play an important role in human locomotion, the fact that human locomotion can emerge from purely reflexive controls increases the attractiveness of using this approach for prosthesis control. The reflex-only paradigm may be easier to design and optimize than the CPG+reflex paradigm for two reasons: First, the reflex connection graph used by Geyer and Herr [2010]'s reflex-only model is much more sparse than that used by Ogihara and Yamazaki [2001] CPG+reflex model. Using a sparse set of reflexes and no CPG reduces the number of parameters that we must tune in order to achieve locomotion. Second, the reflexes in the reflex-only model are functionally motivated, which may increase our intuition about the role of each reflex and assist our ability to tune the model's parameters. This is evidenced by the fact that Geyer and Herr hand tuned the parameters of their model whereas Ogihara and Yamazaki used a genetic algorithm. Moreover, functionally motivated feedbacks used in the reflex-only approach has allowed further research
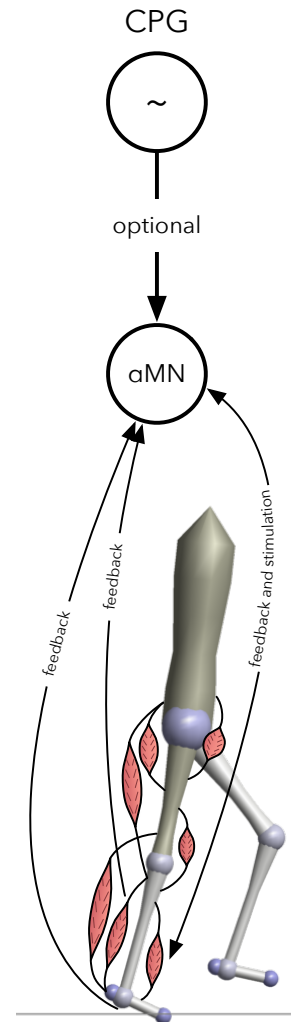
Figure 2.4: Neuromuscular models with reflex feedbacks. The model developed by Ogihara and Yamazaki [2001] activates individual muscles according to the activity of a CPG and proprioceptive reflexes that can involve the muscle itself, other muscles, and ground contact sensing. Geyer and Herr [2010] does away with the CPG and achieves locomotion with only reflex feedbacks.

to extend this model to include swing leg placement [Desai and Geyer, 2013], 3D locomotion, running, speed changes, stair and slope negotiation, turning, and obstacle avoidance [Song and Geyer, 2015].

The robustness properties exhibited by neuromuscular model are especially relevant to our goal of developing a robust prosthesis control that will help transfemoral amputees avoid falls. In Song and Geyer [2015] the author's improve the model's robustness by incorporating reflexes that place the swing leg into target landing angles. The authors optimize this model to achieve a combination of robustness and energy efficiency. The resulting gait can walk on terrains featuring random steps up to ± 6 cm (50 % success rate) and rejects pushes in both the forward and backward directions at various points in the gait cycle. In another work, Murai and Yamane [2011] subject a neuromuscular model, initially trained to match kinematic data of single subject, to impacts during early and late swing. They find the learned model exhibits the elevating and lowering trip response strategies of the biological leg despite not being explicitly trained to do so. These disturbance response characteristics point to reflex control providing the appropriate quasi-static and impedance behaviors.

Neuromuscular Reflexes for Prosthesis Control

Motivated by the robustness and natural gait achievable by neuromuscular reflex control, past research has applied this model to active prostheses and exoskeletons. Eilenberg et al. [2010] applied a simplified version of the control to a powered ankle prosthesis (fig. 2.5). In this work, the neuromuscular model was reduced to a single ankle plantarflexor muscle driven by a positive force feedback reflex during stance. During swing, the control applies torque to dorsiflex the ankle according to a virtual spring damper model. In amputee testing of a prosthesis controlled by the neuromuscular model the control produced ankle kinematics and kinetics similar to those observed in healthy human walking. Significantly, Eilenberg et al. found evidence that the robustness and entrainment properties observed in neuromuscular model simulations may carry over to amputee gait as well. The author's note that the prosthesis automatically adapts torque output when walking on slopes, producing more plantarflexion torque when walking up slopes and less when walking down slopes. Additionally, Markowitz et al. [2011] found that a similar neuromuscular reflex model automatically produced more ankle plantarflexion work as the amputee increased his gait speed.
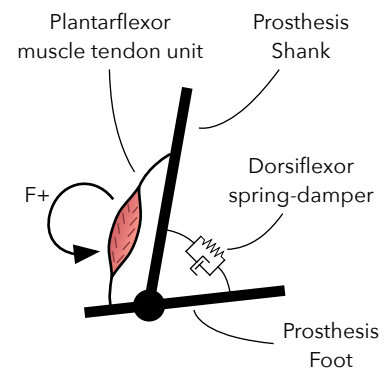
Figure 2.5: Neuromuscular model used by Eilenberg et al. [2010] to control an active ankle prosthesis. During stance, a virtual muscle driven by positive force feedback, generates plantarflexion torque. During swing, a virtual spring damper provides dorsiflexion torque to prevent toe scuffing.

EMG-based Control

The inclusion of user intent recognition via surface electromyography (EMG) signals represents an interesting extension of neuromuscular reflex prosthesis control. In these approaches, muscle activity in the residual limb is directly measured via EMG sensors embedded in the amputee's prosthesis socket. These EMG sensors are then used to control the torque generation of the amputee's leg prosthesis. Because neuromuscular models describe how joint torque is generated in response to muscle activations, a natural approach is to use the EMG signal in reflex pathways in order to activate virtual muscles. This is the approach proposed by Wu et al. [2011]. In this work, Wu et al. control an active transfemoral prosthesis using EMG sensor readings from the residual thigh to activate virtual knee flexor and extensor muscles according to a linearised Hill muscle model. The resulting prosthesis control allowed an intact subject wearing the prosthesis via an able-bodied emulator to achieve nearly normal gait. In a similar approach, Wang et al. [2013] use EMG signals to modify the gain on a positive torque feedback loop (similar to positive force feedback used in Geyer and Herr [2010]) in order to control ankle plantarflexion torque. As seen in healthy human walking, toe off angle and ankle net work increased with increasing walking speed.

These two works have demonstrated that neuromuscular approaches have enabled EMG based control to go beyond its typical application of high-level mode recognition. For example, Huang et al. [2009, 2011], and Hargrove et al. [2015] recognize walking modes, such as level ground walking, ramp and stair ascent, and ramp and stair descent, by training classifiers on features of EMG and mechanical sensor data. In contrast, the EMG + neuromuscular approaches allow the use typically noisy EMG sensor data for low-level continuous control. Wu et al. [2011] and Wang et al. [2013] propose that because EMG + neuromuscular approaches model physiologically plausible feedback loops and dynamics, they may allow amputees to use muscle activations to control their prostheses in an intuitive way.

2.2.3   Conclusion

In summary, simulations and implementations of the neuromuscular reflex control approach have repeatedly demonstrated its ability to generalize to a variety of situations and exhibit robustness to a variety of disturbances. Due to the gait deficits and fall risk transfemoral amputees face, these two properties make this control paradigm very attractive for application to transfemoral prostheses . Moreover, neuromuscular approaches have been successfully extended with EMG sensor feedback from amputees' residual limbs, enabling intuitive

low-level prosthesis control. In contrast, other control approaches for prostheses such as quasi-stiffness control have not demonstrated these properties. Importantly, neuromuscular control addresses challenges 1 and 2 of amputee locomotion (section 1.1.1) as we can implement them via a decentralized, sparse set of reflexes and they allow for dynamism by providing both a quasi-stiffness and impedance response via the dynamics of the stimulated muscle models..

As yet, there have not been any published works applying neuromuscular reflex control to active knee and ankle transfemoral prostheses. Therefore, in this thesis, we work towards this goal with the hope of improving transfemoral amputee gait robustness and naturalness. Chapter 3 will review the details of the particular neuromuscular implementation used in this thesis.

2.3 *Prosthesis Design*

We can trace efforts to build an active knee-ankle prostheses to the seventies when Flowers [1974] created an active knee-ankle prosthesis emulator in order simulate potential control schemes. This prosthesis used a hydraulic actuator capable of producing $90 \, N \cdot m$ of torque and $0.5 \, rev/s$ of no-load speed, sufficient for simulation of passive prostheses. With this device, Donath [1974] tested proportional EMG control, a problem researchers are still investigating today (see section 2.2.2). Indeed, this line of research proved to be far ahead of its time, as most relevant research in active lower-limb prostheses design has occurred only in the last ten years. The recent interest in active knee ankle prostheses has been spurred by hardware improvements that allow designs to approach the strength, speed, and low weight of the biological leg. Enabling technologies include power-dense brushless motors, motor controllers, and lithium-ion batteries, inexpensive microcontrollers and inertial measurement units (IMUs), and strong but light composite materials such as carbon fiber. With these advancements, engineers have successfully designed prostheses to meet or exceed the requirements for walking (table 2.1).

In this section, we review a number of recent prosthesis designs and analyze their ability to enable dynamic locomotion (challenges 1 and 2 of transfemoral prosthesis locomotion). To address this challenge, prostheses should be able to regulate their output joint torques and behave as though they have inertial properties similar to that of a normal human leg. This will ensure that the prosthesis will emulate the energy efficient gaits of normal walking and remain compliant to unforeseen disturbances and uneven terrain.

	Ankle Max	Knee Max
Velocity	$0.72 \, rev/s$	$1.17 \, rev/s$
Torque	$130 \, N \cdot m$	$57 \, N \cdot m$
Power	$350 \, W$	$120 \, W$

Table 2.1: Required knee and ankle torque, velocity, and power for walking ($1.40 \, m/s$ average speed, scaled to $85 \, kg$ subject, data from Winter [2009])

2.3.1   Direct Drive Transfemoral Prostheses

The most common approach for active transfemoral prosthesis design employs electric motors, coupled to transmissions, that directly drive the knee and ankle joints. The transmissions may utilize a combination of gears, chains, belts, ball screws, and four-bar-mechanisms in order to increase the torque output of the actuator, at the expense of speed, in order to satisfy the requirements listed in table 2.1. A successful line of transfemoral prostheses following this design paradigm comes from Vanderbilt university. The first prosthesis in this line fig. 2.6a used a pair of ball screw transmissions and brushless motors capable of 200 W of continuous power output to drive its knee and ankle joints [Sup et al., 2009].

With these actuators, the knee motor can achieve the required peak torque and peak power intermittently (table 2.1). However, the ankle motor may be overly stressed due to the high requirements of walking. To remedy this, this prosthesis includes of a unidirectional parallel spring in the ankle that reduces the required ankle motor torque. As shown in figure fig. 2.7, during level ground walking, a linear torsion spring accounts for a significant portion of the ankle's torque versus angle relationship. Therefore, incorporating a spring into the ankle offloads this portion of the torque from the motor. The ankle motor only needs to provide the delta between the desired output torque and the linear spring. As a result, the spring reduces motor energy consumption, heat generation, and transmission wear.

Further improvements resulted in two more generations of prostheses (figs. 2.6b and 2.6c) [Lawson et al., 2013, 2014]. These versions replaced ball screw transmissions with a multi-stage belt/chain due to the improved packaging and reduced noise and wear they afford (Michael Goldfarb, personal communication, September 18, 2013). With these prostheses, researchers have extensively tested a variety of control strategies including quasi-stiffness control [Sup et al., 2009, 2011, Lawson et al., 2013, 2014, Lenzi et al., 2014b], EMG-based control [Ha et al., 2011, Varol et al., 2010], minimum jerk trajectory following [Lenzi et al., 2014a], and virtual constraint control [Gregg et al., 2014].

Additional prostheses in the direct drive category include AMPRO [Zhao et al., 2016], and a commercially available active knee and ankle prostheses: the Össur Power Knee and Proprio Foot. The AMPRO prosthesis features two 374 W motors coupled to Harmonic Drive transmissions. Zhao et al. [2016], use this prosthesis to asses the merits of a virtual constraint controller. The Össur Power Knee features an electric motor that can provide torque to facilitate sit-to-stand motions, stair climbing, and active extension and flexion
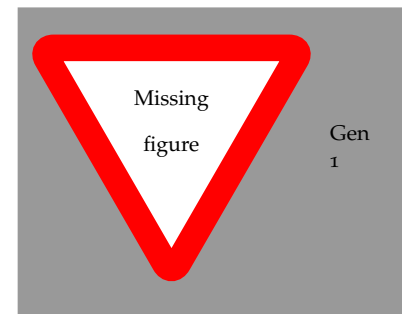
(a) Generation 1 used ball screw transmissions, 200 W brushless motors, and a unidirectional parallel spring in the ankle that reduced motor torque requirements [Sup et al., 2009].
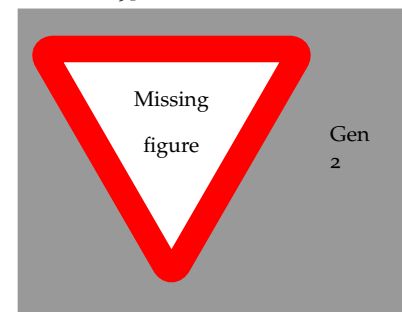
(b) Generation 2 replaced ball screws with custom gear-based transmission that is less noisy and more durable [Lawson et al., 2013].
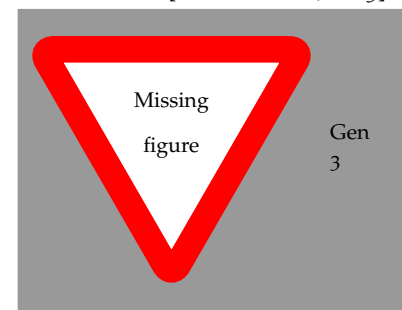
(c) Generation 3 features a modular design with separable knee and ankle units [Lawson et al., 2014].

Figure 2.6: Vanderbilt University's Robotic Transfemoral Prostheses.

during walking. The Proprio Foot also features electric actuation that allows it to adapt to terrain and dorsiflex the ankle during swing to help avoid trips.

Torque Control Strategies for Direct Drive Prostheses

In order to achieve dynamic locomotion capabilities, it is crucial that prosthesis designs allow for closed loop control of torques. To do this control system must be able to accurately measure the torque at the joint output. There are two main strategies for torque measurement used by direct drive prostheses.

The first strategy is to measure the current draw of the motors windings, which is related linearly to the motor torque. One can then multiply this measurement by the gear ratio to obtain an estimate of the output joint torque. This is the method used by Generations 2 and 3 of the Vanderbilt prosthesis as well as the AMPRO prosthesis. The benefit of this method is that it utilizes existing hardware and allows one to use high frequency current control modes of motor drivers. However, a drawback of this method is that it measures the torque before the transmission. Consequently, it does not account for frictional losses, which can be difficult to model, especially for geared systems. A strategy that deals with this problem is to install load cells in series with the motor after the transmission, as was done on Generation 1 of the Vanderbilt prosthesis. With this method, the closed-loop control can compensate for frictional losses as they are included in the torque measurement.

However, this method may still not address a second problem: sluggish passive dynamics caused by reflected inertia and damping. Reflected inertia refers to the apparent magnification of motor rotor and gearing inertia on the outside of gearbox. We can derive this effect through Newton's second law for the geared motor

$$J_i \ddot{\theta}_i = \tau_i - b_i \dot{\theta}_i. \tag{2.5}$$

Here, θ and its derivatives refer to angular states of the motor, b is the damping constant, J is the inertia and τ is the motor torque. We use subscript i to refer to these quantities as seen before the gear reduction, and subscript o to refer to those quantities reflected outside of the motor. Plugging in $\theta_i = n\theta_o$ and $\tau_i = \frac{1}{n}\tau_o$, where n is the gear ratio, and multiplying through by n yields

$$J_i n^2 \ddot{\theta}_o = \tau_o - b_i n^2 \dot{\theta}_o \tag{2.6}$$

$$\implies \quad J_o \ddot{\theta}_o = \tau_o - b_o \dot{\theta}_o. \tag{2.7}$$

These equations show that the inertia and damping of the motor rotor are amplified by the square of the gear ratio. As prostheses may often use gear ratios in excess of 100:1, this effect can be substantial.
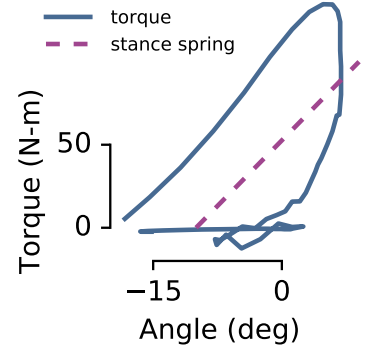

Figure 2.7: Torque vs angle relationship for the ankle during level ground walking. A linear spring relationship captures a significant portion of ankle function during stance. Data from Winter [2009] scaled to 85 kg subject.

	Knee	Ankle
rotor inertia	$0.035\,\mathrm{kg \cdot cm^2}$	$1.210\,\mathrm{kg \cdot cm^2}$
gear ratio	176:1	115:1
reflected inertia	$0.11\,\mathrm{kg \cdot m^2}$	$1.6\,\mathrm{kg \cdot m^2}$
human inertia	$0.66\,\mathrm{kg \cdot m^2}$	$0.019\,\mathrm{kg \cdot m^2}$
percent increase	17%	8400%

Table 2.2: Estimated reflected inertia at knee and ankle joints of Generation 3 Vanderbilt Prosthesis [Lawson et al., 2014]. Motor data taken from Maxon Motors Catalog[Motor, 2016b,a] Knee reflected inertia compared to inertia of human shank and foot about knee. Ankle inertia compared to human foot about its center of mass. Human inertias estimated from Winter [2009] for an 85 kg, 1.7 m tall person.

For example, table 2.2 shows the calculated reflected inertias of the Maxon Motors used in Generation 3 of the Vanderbilt prosthesis and compares the values to the estimated inertia of the shank and foot about the knee and the foot about its center of mass. We see that at the knee, the reflected inertia is roughly 17% of that of the human shank and foot. In practice, this value is likely several times higher after including the inertia of the encoder, bearings, and gearing. Consequently, we can estimate that the reflected inertia may be on the order of the leg itself. At the ankle, the reflected inertia of the rotor alone is several orders of magnitude more than that of the foot and more than twice that of the shank and foot. When we also consider reflected damping and friction, the dynamics of prosthesis system may be significantly slower than assumed.

The increase in joint impedance created by transmissions could present an issue when attempting to execute dynamic behaviors involving impact such as running or trip recovery. In an impact event, the impulse will move through the system at the speed of sound through metal, roughly $6420\,\mathrm{m/s}$ for aluminum [Lide, 2004]. If the prosthesis is 0.5 m long, the shock will traverse its length in 0.00008 seconds. This is about 10 times faster than the typical 1000 Hz control frequency of prosthesis control systems, rendering closed loop torque control with load cells unresponsive. The impact shock could cause damage to gearing and discomfort for the amputee.

2.3.2 *Design of Dynamic Prostheses*

In contrast to the direct drive actuation discussed in the previous subsection, prostheses that employ series elastic actuation may be better poised to achieve dynamic locomotion [Pratt and Williamson, 1995]. This actuation scheme (illustrated in fig. 2.8) aims to solve the torque measurement and impedance amplification caused by transmissions by placing a spring in series with the actuator. Measuring the deflection of the spring allows for accurate closed-loop control of the joint torque. Moreover, the spring low-pass filters external impulses, granting the control system more time to move the motor rotor in response to the external load. Due to these properties, designers have integrated series elastic actuators into a number of bipedal robots

that seek to achieve dynamic locomotion such as M2V2 [Pratt and Krupp, 2008] and ATRIAS [Grimes, 2013].

Series elastic actuators have found use in a variety of transtibial and transfemoral prostheses. We can further split these applications into two categories, those that optimize the spring stiffness for control bandwidth subject to shock tolerance and those that optimize spring stiffness to optimize efficiency.

Springs for Bandwidth and Shock Tolerance

Adding a spring between the gear and load introduces additional dynamics between external torques and torques applied to the gearbox as external torques must physically displace the load before they generate torque on the motor. This property can improve the shock tolerance of SEA actuators over that of direct drive motors [Robinson, 2000]. However, by the same token, the SEA also introduces additional dynamics between motor torque and load torque, hence reducing force control bandwidth. Therefore, a trade-off exists between the compliance of the actuator and speed with which it can generate desired torques.

Au et al. [2007], Au and Herr [2008] design powered ankle prostheses with this trade off in mind. In these publications, the authors find that using an SEA spring soft enough to protect the ball screw transmission results in insufficient closed loop torque control bandwidth. To overcome this shortcoming, the authors incorporate a parallel spring into the ankle as was done for some of the knee and ankle prostheses discussed in section 2.3.1. Because the parallel spring offsets the motor's torque requirements, Au and Herr find that it also improves the bandwidth of the system from 4 Hz to 20 Hz, thereby exceeding the requirement for walking.

Caputo and Collins [2013] also used series elastic actuators in a robotic prosthesis testbed. This system uses a large, 1.61 kW offboard motor connected to a light-weight prosthesis end-effector via a Bowden cable transmission. The Bowden cable applies forces to one end of a fiberglass leaf spring strain gauges measure its deflection. The author's note that the series springs isolate the prosthesis end effector from the motor's rotor inertia. With this system the author achieve a large peak output torque (175 N · m) and high bandwidth (17 Hz), allowing them to rapidly test the effects of different control strategies and emulate prosthesis hardware [Caputo et al., 2015].

Springs for energy efficiency

Designers can also tune series elasticity in order to improve energy efficiency by mimicking the role of tendons in the biological human

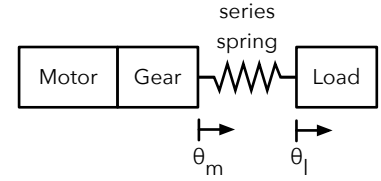Figure 2.8: Series elastic actuation inserts a spring between the gear output and the load (here drawn as linear actuator for simplicity). Torque is measured via the spring deflection, $\tau = k(\theta_l - \theta_m - \theta_0)$ where τ is the output joint torque, k is the spring constant, and θ_l and θ_m are the load and motor positions and θ_0 is the spring's rest length.

leg. In the human ankle, the Achilles tendon, which is in series with the ankle plantarflexor muscles, stores energy throughout stance and releases it just prior to toe-off, producing a surge of mechanical power. During this process, the ankle plantarflexor muscles hold the proximal end of the tendon nearly stationary via isometric contraction. This kind of length-preserving muscle contraction consumes relatively little metabolic energy compared to concentric or length-shortening contractions [Rall, 1984]. Consequently, ankle elasticity helps store and release energy, thereby improving metabolic cost of walking [Sawicki et al., 2009].

Similarly, the SPARKy prosthesis uses a *Robotic Tendon* comprised of helical springs in series with the motor to store and release energy ankle energy during stance [Hitt et al., 2007, Bellman et al., 2008, Holgate et al., 2008]. Adding a series spring changes the ankle motor movement to that required to generate desired output torque given the stiffness of the spring and trajectory of the ankle joint[4]. Therefore, with a properly tuned series spring the design reduces motor movement and thus required motor power from 250 W to 77 W [Hitt et al., 2007].

[4] $\theta_m = \theta_l - \tau/k - \theta_0$, where τ is the desired ankle torque, θ_l is the ankle trajectory, and k and θ_0 are the spring stiffness and offset

Transfemoral prosthesis designs have also sought to use springs in the knee joint in order to improve energy efficiency. However, these prostheses require more sophisticated designs due to the complex behavior of the knee. Whereas a single spring relationship explains a significant portion of ankle joint behavior (fig. 2.7), as shown in fig. 2.9, the knee joint requires two springs: one for early stance and one for pre-swing and swing. Two prostheses that tackle this design problem are AAAKP (agonist-antagonist active knee prosthesis) [Martinez-Villalpando et al., 2008, 2011] and the CSEA (clutchable series elastic actuator) knee [Rouse et al., 2014, 2015].

The AAAKP prosthesis uses two unidirectional springs, one for extension and one for flexion, each in series with its own actuator. With this setup, AAAKP is able to store energy during the knee flexion phase just after heel strike, and transfer it to a flexion spring for use during pre-swing and swing. The prosthesis consumes just 5.6 J/stride. However, the downside of this design is inefficient use of actuator mass, as two electric motors are required, one for extension and one for flexion.

A second concept is to use a series elastic actuator with a clutch on the motor [Rouse et al., 2014, 2015] The clutch saves energy by holding the motor side of the series spring stationary while the spring is loaded in early stance; no electrical energy is consumed holding the rotor in place. In this design the spring-like behavior of the knee during swing is reproduced by the electric motor alone unlike in the AAAKP prosthesis. Despite this, the CSEA knee consumes less en-
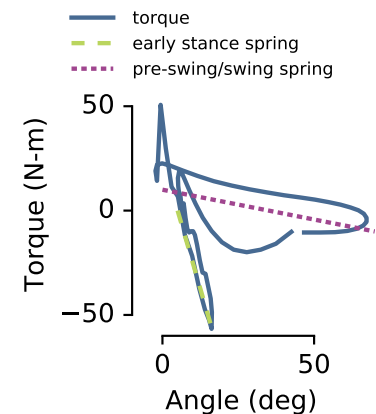

Figure 2.9: Torque vs angle relationship for the knee during level ground walking. Knee displays more complicated functionality than the ankle (see fig. 2.7), with two distinct springs need to explain early stance and pre-swing/swing behavior. Data from Winter [2009] scaled to 85 kg subject.

ergy than the AAAKP, just 3.6 J/stride. Moreover, the simplified design of the CSEA has a mass of 2.7 kg vs 3.6 kg for the AAAKP.

A potential drawback of SEA designs that are tuned for energy efficiency is that they typically tune tune the spring stiffness to match observed quasi-stiffness of the biological joint during a certain phase of the gait. However, this stiffness value is not necessarily that which maximizes torque control bandwidth. Therefore, while prostheses tuned for efficiency can consume less energy, which is desirable for a product needing long battery life, they may not represent the most versatile design for evaluating new control ideas or different gait modes.

2.4   Stumble Recovery for Prostheses

The prosthesis controls we reviewed in sections 2.1 and 2.2 primarily sought to reproduce typical walking kinematics and dynamics. Some control strategies, such as neuromuscular reflex control (section 2.2.2) also demonstrated the ability to generalize to sloped walking and changes in speed by producing more push off work in these situations [Eilenberg et al., 2010, Markowitz et al., 2011]. However, it is not clear that the low-level reflexes in the neuromuscular control model will generate trip recovery responses, which in human control likely utilize more complex supraspinal and cortical reflexes [Eng et al., 1994, Schillings et al., 2000, Hofstad et al., 2009]. We therefore seek to improve upon neuromuscular control's inherent stability by augmenting it with explicit trip detection and recovery actions.

As discussed in section 1.1, falling and the fear of physical activity it engenders are two major issues amputees face [Miller et al., 2001]. Avoidance of physical activity can potentially cause deterioration of strength, balance and control, which may lead to further inactivity, debilitation, and social isolation. Currently, the microprocessor controlled, mechanically-passive prostheses feature trip recovery modes that "lock" or highly damp knee movement. However, Bellmann et al. [2010] show that these modes fail to adequately respond to trips during a large portion of swing due to knee buckling at touchdown. Moreover, it is unclear that passive, locking responses are intuitive for amputees or coordinate well with innate trip recovery responses, which can require positive joint power [Cordero et al., 2005]. However, the advent of active transfemoral prostheses give us the opportunity to replicate amputee's preferred responses, which will hopefully yield more effective and intuitive fall-prevention actions.

2.4.1   Responses to Trips

Able-bodied persons primarily use two strategies to recover from trips to their swing legs: When the tripped in early swing, people usually use an *elevating strategy*, in which the knee is actively flexed to lift the foot over and in front of the obstacle. In late swing, people typically use a *lowering strategy*, in which knee extensor muscles rapidly bring the foot in contact with the ground in front of the obstacle [Eng et al., 1994]. In response to mid-swing trips, people may use either strategy [Schillings et al., 2000]. Finally, the *delayed lowering* can also be used in early swing. This strategy is an aborted attempt at an elevating strategy, followed by a lowering strategy, and is used when the toe catches on the obstacle [Eng et al., 1994].

Interestingly, Shirota et al. [2015] show that transfemoral amputees using mechanically-passive prostheses utilize these same strategies despite the lack of control and positive power production at the knee joint. Amputees compensated for these deficiencies and achieved elevating, lowering, and delayed lowering foot trajectories via movements of the hip and sound side leg. The lack of sensory feedback information from the prosthesis leg to the nervous system did not seem to impede utilization of these strategies. Consequently, the authors hypothesize that mimicking able-bodied responses to trips may also be intuitive for amputee subjects.

While amputees using mechanically-passive prostheses exploit the same strategies as able-bodied subjects for trip recovery, they do not use these strategies in the same proportions during the phases of swing as do able-bodied subjects. Amputees typically use elevating strategies less frequently and lowering strategies more frequently. This difference increases when the prosthesis is the stance leg, and the intact leg is tripped. A possible reason for decreased reliance on the elevating strategy may stem from the inability of mechanically-passive prostheses to produce positive joint power. Cordero et al. [2005] show that in an elevating strategy, positive power is required in the swing-leg's knee joint in order to rapidly flex the knee to achieve obstacle clearance. Likewise, Pijnappels et al. [2004] show that powered stance leg push-off helps raise the foot during the elevating strategy. Empowering transfemoral prostheses with active joints may help amputees more easily realize the elevating strategy, normalize amputee trip recovery strategy selection, and allow them to recover from a larger range of disturbances.

2.4.2   Trip Detection and Classification

Human responses to gait disturbances likely involve signal processing at the supraspinal and cortical level. This is evidenced by

the relatively high latency ($>$ 100 ms) of EMG signals relevant to the utilized strategy, the utilization of both elevating and lowering strategies in mid-swing, the existence of the delayed lowering strategy [Schillings et al., 2000], and the inconsistent resolution of motor redundancy during the lowering strategy [Eng et al., 1994]. Furthermore, Hofstad et al. [2009] found that latencies are further increased for amputee subjects executing obstacle avoidance tasks, suggesting that amputee trip recovery may require additional data processing and cognitive control as compared to able-bodied persons.

A control system that seeks to be intuitive and effective for amputees by mimicking their responses to trips needs to be able to model these complexities. As a result, researchers have relied on data-driven and machine learning approaches to detect and classify trips so that prostheses can take the appropriate actions. All systems designed to date use a two-layer classification scheme, where the first layer distinguishes trips from normal walking, and the second layer classifies the recovery strategy as either elevating or lowering. The first such system by Lawson et al. [2010] used Fast Fourier Transform features of data collected from six accelerometers placed on the lower limb. To collect training data, the author's outfitted healthy subjects with sensors, and randomly subjected them to trips. They classified stumbles from normal walking via a threshold on power between 10 and 40 Hz and classified elevating versus lowering strategies based on the root-mean-squared thigh acceleration in a 50 ms window before the stumble. Zhang et al. [2011] further add EMG sensors to the trip detection system, and employ outlier detection methods so that the trips were not required in the training dataset. They find EMG sensors improve the false alarm rate, at the expense of classification latency. However, the false alarm rate is still quite high, corresponding to an incorrect positive classification every 1.6 min. Finally, Shirota et al. [2014] use linear discriminant analysis on kinematic features from the tripped leg. They find evidence supporting the use of the two-stage classification scheme, and identify the optimal update frequency and length for the window in which they compute features.

A major drawback of these previous works is that they report error rates based on offline validation results; *i.e.* they collect data from subjects who are responding to trips and then evaluate how well the classifier would have performed on the collected data. This is fundamentally different than online validation, in which one reports the error rate obtained when using the learned classifier to control the system. Previous work on a classifier for recognizing gait modes such as level walking and stair and ramp ascent and descent found that online error rates were significantly higher than offline error

rates [Hargrove et al., 2015]. As we discuss in section 5.2, it is likely
this trend will hold true for stumble classification as well.

3
Neuromuscular Model

In this thesis we intend to investigate the ability of neuromuscular reflex control to improve amputee gait robustness. To this end, here we provide a more detailed review the neuromuscular model components on which we base our prosthesis control. Four parts comprise the model: a mechanical simulation environment we use to obtain simulation results (section 3.1), biological motors modeled by the hill muscle model that apply torques to joints (section 3.2), and finally functionally-motivated stance (section 3.3) and swing (section 3.4) reflexes that implement the key behaviors required for walking.

3.1 Mechanical Model

To obtain the simulation results we present in section 4.2, we construct a mechanical model in the Matlab Simscape Multibody environment similar to those presented in Geyer and Herr [2010], Song et al. [2013], Song and Geyer [2015]. This model represents the seven link biped in fig. 3.1 and includes two legs with thigh, shank, and foot segments as well as a lumped head-arms-trunk (HAT) segment. Table 3.1 lists the segment lengths, center of mass and joint locations measured from the distal end, masses, and inertias that approximate those of a 80 kg, 2.0 m tall person.

The mechanical model interacts with the environment through ground reaction forces on the toes and balls of the feet. Specifically, we use a 2-dimensional reduction of the 3D ground contact model
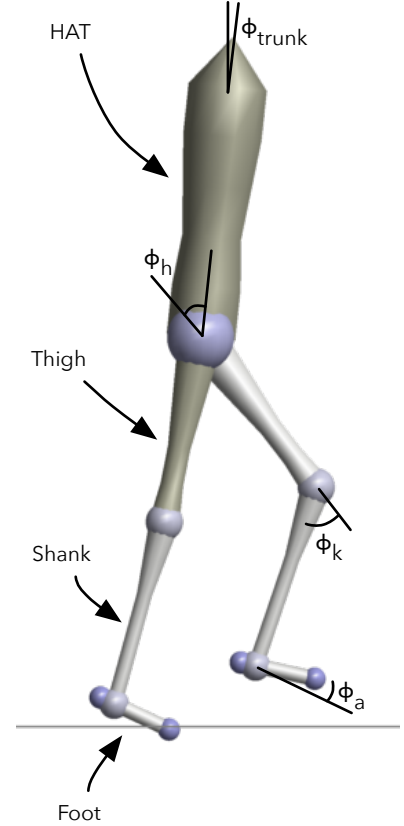
Figure 3.1: The skeletal model we use to simulate neuromuscular reflex control. The model consists of seven segments: left and right feet, shanks, and thighs, as well as a lumped head-arms-trunk (HAT) segment. Flexion joint angles are positive, extension joint angles are negative, and the zero angle configuration represents standing.

	Feet	Shanks	Thighs	HAT
l (cm)	20	50	50	80
d_{COM} (cm)	14	30	30	35
d_{Joint} (cm)	16	50	50	
m (kg)	1.25	3.5	8.5	53.5
J (kg)	0.005	0.05	0.15	3

Table 3.1: Segment lengths (l_s), center of mass (d_{COM}) and joint (d_{Joint}) locations measured from the distal end, masses (m), and inertias (J) approximated from Günther and Ruder [2003].

presented in Song and Geyer [2013] to calculate forces in the normal and tangential directions with respect to the terrain. In the normal direction the force is

$$F_\mathrm{n} = k_\mathrm{n} \Delta n_c (1 + \dot{n}_c)(\Delta n_c > 0)\left(\dot{n}_c/v_\mathrm{max} > -1\right), \qquad (3.1)$$

where $k_\mathrm{n} = 78.45\,\mathrm{N/mm}$ is the stiffness coefficient in the normal direction and Δn_c and $\dot{n}_c$ are the normal penetration in the normal direction and velocity. The form of the normal force is inspired by Günther and Ruder [2003], Scott and Winter [1993] and represents a linear spring with multiplicitive damping. $v_\mathrm{max} = 3\,\mathrm{cm/s}$ represents the maximum recovery velocity of the ground. If $\dot{n}_c$ exceeds this velocity ground contact is lost.

In the tangential direction, a state machine switches between two force models representing sliding and static friction. Sliding friction is given by

$$F_\mathrm{t,slide} = -\operatorname{sign}\left(\dot{t}_c\right)\mu_\mathrm{slide}F_n \qquad (3.2)$$

while static friction is given by

$$F_\mathrm{t,static} = -k_t \Delta t_c \left(1 + \operatorname{sign}\left(\Delta t_c\right)\frac{\dot{t}_c}{v_\mathrm{max}}\right), \qquad (3.3)$$

where Δt_c is the penetration in the tangential direction $\dot{t}_c$ is the penetration velocity, $\mu_\mathrm{slide} = 0.8$ is the sliding coefficient of friction, and $k_\mathrm{t} = 78.45\,\mathrm{N/mm}$ is the stiffness coefficient in the tangential direction.

The contact model begins in the sliding mode and switches to the static mode if $\dot{t}_c < 11\,\mathrm{cm/s}$. It switches back to the sliding mode when $|F_\mathrm{t,static}| < \mu_\mathrm{static}|F_n|$, where $\mu_\mathrm{static} = 0.9$.

Finally, the biped skeletal model includes soft joint limits to represent the skeletal joint limits on the knee, ankle, and hip joints. The functional form form the soft limit joint torque is identical to that of the normal ground reaction force given by eq. (3.1).

$$\tau_{jl} = k_{jl} \Delta \phi_{jl} (1 + \dot{\phi}_{jl})(\Delta \phi_{jl} > 0)\left(\dot{\phi}_{jl}/\dot{\phi}_\mathrm{max} > -1\right), \qquad (3.4)$$

where $k_{jl} = 0.3\,\mathrm{N \cdot m/deg}$ is the joint stiffness $\Delta \phi$ and $\dot{\phi}_{jl}$ are the joint limit penetration angle and velocity respectively, and $\dot{\phi}_\mathrm{max} = 1\,\mathrm{deg/s}$ is the maximum joint limit retraction velocity. Table 3.2 lists the engagement angles for the joint limits.

To obtain simulation results, we simulate the mechanical system with the ode15s variable step solver. We set the maximum step size to $10\,\mathrm{ms}$, relative error tolerance to 10^{-4}, and abolute error to 10^{-6}.

Joint	ext. lim.	flex lim.
hip		50
knee	5	
ankle	-40	20

Table 3.2: Joint limits for the hip, knee, and ankle joints listed in degrees. Positive joint angles represent flexion and negative joint angles represent extension (see fig. 3.1).

3.2   Hill Muscle Models

Our proposed transfemoral prosthesis control is comprised of biological muscle actuators that are stimulated according to hypothesized reflex pathways. Specifically, we use a Hill-type *muscle tendon unit* (MTU) developed in Geyer and Herr [2010]. It is comprised of a contractile element (CE) that represents muscle fibers and produces force when activated, a parallel elastic (PE) element that represents the stiffness of the collagen tissue between muscle fascicles, and series elastic (SE) element that models tendon stretch. Figure 3.2 shows the arrangement of these elements. Note that the PE and SE both are unidirectional springs with engagement lengths of l_{opt} and l_{slack} respectively.

The CE generates force according to

$$F_{CE} = F_{max} A \, f_l \left(l_{CE} \right) f_v \left(v_{CE} \right). \tag{3.5}$$

In this equation, the force generated by the CE (F_{CE}) is the maximum isometric (constant length) force (F_{max}) multiplied by activation (A), the force-length ($f_l(\cdot)$), and force-velocity ($f_v(\cdot)$), relationships of the CE. The activation A is a low-pass filtered version of the stimulation signal muscle $S(t)$ generated by the muscle reflexes we will detail in the next section. This filter, given by $A(t) = S - \tau \dot{A}(t)$ with time constant τ, represents the diffusion dynamics of calcium ions that activate binding sites in the muscle fibers.

The binding sites are where overlapping actin and myosin filaments attach and generate pulling force. The contractile element length of l_{opt} corresponds to maximum overlap between these filaments. Therefore, as as the muscle length moves away from l_{opt}, its force production capacity decreases leading to the force-length relationship shown in fig. 3.3. We model the force-length relationship via a bell curve

$$f_l \left(l_{CE} \right) = \exp \left(\ln(0.05) \left| \frac{l_{CE} - l_{opt}}{w l_{opt}} \right|^3 \right). \tag{3.6}$$

The velocity-dependent filament attachment probabilities give rise to a force-velocity relationship shown in fig. 3.4. The following expression captures this relationship.

$$f_v \left(v_{CE} \right) = \begin{cases} \frac{v_{max} - v_{CE}}{v_{max} + K v_{CE}}, & \text{if } v_{CE} < 0 \\ N + (N - 1) \frac{v_{max} + v_{CE}}{7.56 K v_{CE} - v_{max}}, & \text{if } v_{CE} \geq 0 \end{cases} \tag{3.7}$$

In this expression, K is a shape parameter and N determines the force amplification when the contractile element is lengthening. The force-velocity relationship acts as a multiplicative damper causing the
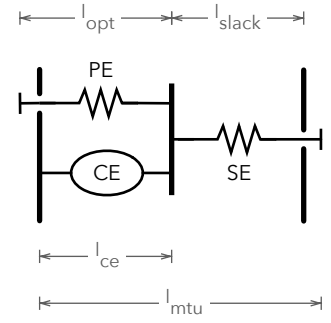

Figure 3.2: Hill-type muscle tendon unit with contractile element (CE), parallel elasticity (PE), and series elasticity (SE).
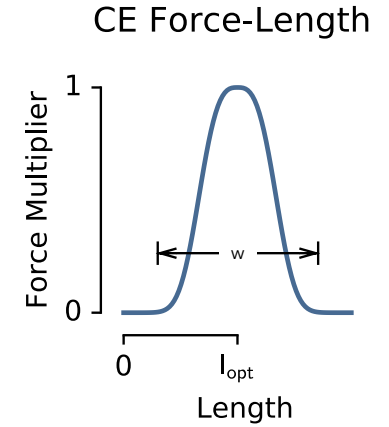
CE Force-Length

Figure 3.3: Force-length relationship of the CE.
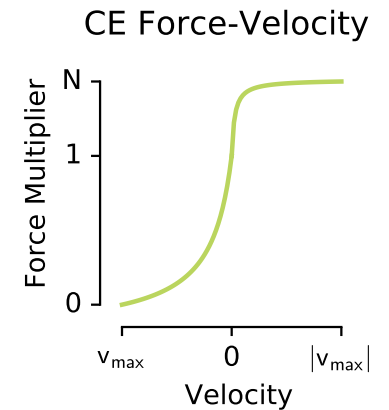
CE Force-Velocity

Figure 3.4: Force-velocity relationship of the CE.

Param	Value	Param	Value
τ	0.1 s	l_{opt}^{ham}	0.10 m
w	0.56	v_{max}^{ham}	-1.2 m/s
K	5	F_{max}^{ham}	3000 N
N	1.5	l_{slack}^{ham}	0.31 m
ϵ_{PE}	w		
ϵ_{SE}	0.04		

Table 3.3: Neuromuscular parameters for shared entities (left) and the hamstring muscle (right)

CE to produce more contractile force when it is lengthening and less as it extends.

We model both passive elements, the PE and SE, using the same functional form representing a unidirectional, stiffening spring, the behavior of which is shown in fig. 3.5. The expressions for the elastic force produces by these elements are

$$F_{PE}\left(l_{CE}\right) = F_{max} \left(\frac{l_{CE} - l_{opt}}{\epsilon_{PE} l_{opt}} \right)^2 \left(l_{CE} > l_{opt}\right) \tag{3.8}$$

$$F_{SE}\left(l_{SE}\right) = F_{max} \left(\frac{l_{SE} - l_{slack}}{\epsilon_{SE} l_{slack}} \right)^2 \left(l_{SE} > l_{slack}\right). \tag{3.9}$$

The left-hand side of table 3.3 lists the parameters common among all seven muscles of each leg of the neuromuscular model. On the right-hand side of the table, we list four muscle-specific parameters for hamstrings muscle. For a complete list of muscle parameters please refer to Song and Geyer [2015].

The full biped model, shown in fig. 3.6, includes seven Hill-Type muscle-tendon units: soleus, gastrocnemius, tibialis anterior, vastus, hamstring, hip flexors, and gluteus. The length of these MTUs is related to the joint angles according to the variable-length moment arms $r_{mtu}^j\left(\text{Œ}^j\right)$ for each muscle about each joint. For example, the

Figure 3.5: PE and SE force length relationship. For the PE, $l_{ref} = l_{opt}$ and $\epsilon_{ref} = \epsilon_{PE}$. Likewise, for the SE, $l_{ref} = l_{slack}$ and $\epsilon_{ref} = \epsilon_{SE}$.

Figure 3.6: Biped walking model with labeled muscles.

length of a biarticular muscle spanning joints j and k is

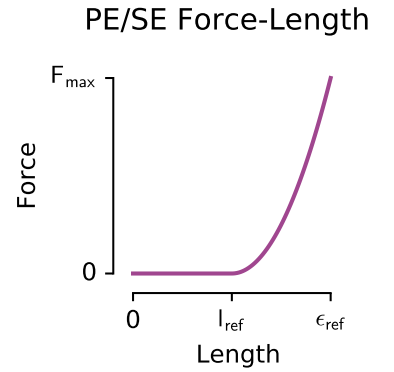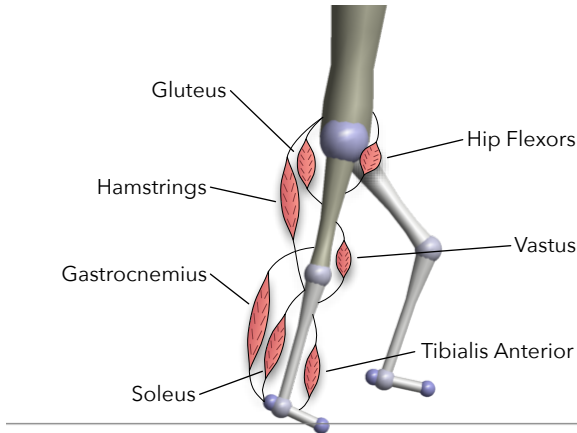$$l_{\text{mtu}} = l_{\text{opt}} + l_{\text{slack}} + \rho \left(\int_{\phi_0^j}^{\phi^j} r_{\text{mtu}}^j \left(\phi^j \right) \, \mathrm{d}\phi^j + \int_{\phi_0^k}^{\phi^k} r_{\text{mtu}}^k \left(\phi^k \right) \, \mathrm{d}\phi^k \right).$$

$$(3.10)$$

Where ρ is a parameter that approximates the effect of the pennation angle of the muscle fibers. The variable length moment arms also govern the torque a muscle produces about a joint according to

$$\tau_{\text{mtu}} = r_{\text{mtu}}^j \left(\phi^j \right) F_{\text{mtu}}.$$

$$(3.11)$$

3.3 Stance Reflexes

During stance, hypothesized reflex feedback pathways stimulate the muscles of the leg. In general, a linear feedback law governs the stimulation $S^m(t)$ of muscle m,

$$S^m(t) = S_0^m + \sum_n G_n^m \text{Pro}_n(t - \Delta t_n),$$

$$(3.12)$$

where S_0^m is a constant pre-stimulation, $\text{Pro}_n(t - \Delta t_n)$ is the time-delayed proprioceptive signal from muscle n, and G_n^m is the gain on that signal. The proprioceptive signal can take the form of force feedback, $F_n^m(\cdot)$, which uses the time delayed tendon force, or length feedback, $L_n^m(\cdot) = l_{\text{CE},n}(\cdot) - l_{\text{off},n}$, which uses the difference between the length of the contractile element and an offset length l_n^{off}.

The time delay we apply to proprioceptive signals estimate the round-trip neural signal transmission delay of afferent signals from muscle spindles and Golgi tendons to the spine and efferent signals back to the muscles. For ankle muscles, the soleus, tibialis anterior, and gastrocnemius, the time delay is $\Delta t_n = 20\,\text{ms}$. For knee muscles, the vastus and hamstrings, it is $\Delta t_n = 10\,\text{ms}$. For the hip muscles, the hamstrings, gluteus, and hip flexors, the time delay is $\Delta t_n = 5\,\text{ms}$. We will denote time delayed signals using $t_l = t - 20\,\text{ms}$, $t_m = t - 10\,\text{ms}$, and $t_s = t - 5\,\text{ms}$.

The reflexes encode several key functions of legged locomotion: generating compliant leg behavior, preventing knee overextension, and balancing the trunk.

The reflexes achieve the first function, generating compliant leg behavior, via positive force feedback on the monoarticular leg extensors: the soleus, vastus, and gluteus. For example, the reflexes stimulated the vastus in part by

$$S^{\text{vas}}(t) = S_0^{\text{vas}} + G_{\text{vas}}^{\text{vas}} F_{\text{vas}}(t_m) + \dots.$$

$$(3.13)$$

To implement the second function, preventing knee overextension, the reflex control uses two strategies. First, positive force feedback

of the biarticular gastrocnemius and hamstrings muscles helps counteract the tendency for knee overextension caused by ankle plantarflexion and hip extension torques, respectively. For example, the gastrocnemius has a force feedback reflex,

$$S^{\text{gas}}(t) = S_0^{\text{gas}} + G_{\text{gas}}^{\text{gas}} F_{\text{gas}}(t_l) , \tag{3.14}$$

that flexes the knee as it contributes to anklep plantarflexion. The hamstring also has a positive force feed back

$$S^{\text{ham}}(t) = S_0^{\text{ham}} + G_{\text{ham}}^{\text{ham}} F_{\text{ham}}(t_s) + \dots \tag{3.15}$$

that counteracts knee flexion caused by hip extension. Also, the hamstring force feedback helps prevent hip flexion caused by heel-strike.

A second mechanism further protects the knee by inhibiting the vastus stimulation in proportion to knee extension beyond a threshold, resulting in the complete vastus stimulation

$$S^{\text{vas}}(t) = S_0^{\text{vas}} + G_{\text{vas}}^{\text{vas}} F_{\text{vas}}(t_m) - k_\phi \left(\phi_k(t_m) - \phi_k^{\text{off}} \right)$$
$$\times \left(\phi_k(t_m) < \phi_k^{\text{off}} \right) (\dot{\phi}_k(t_m) < 0) \tag{3.16}$$

where ϕ_k^{off} is the angle beyond which the vastus is inhibited.

The reflexes achieve the final function of balancing the trunk by proportional-derivative control that produces stimulations for the hip muscles (hip flexors, gluteus, and hamstrings) to stabilize the trunk at a reference lean. Because muscles can only provide pulling force, the proportional derivative control signal is distributed as hip flexor stimulation if the signal represents flexion torque and as simultaneous stimulation for the gluteus and hamstrings if it represents hip extension torque. For example, the complete hamstrings stimulation becomes

$$S^{\text{ham}}(t) = S_0^{\text{ham}} + G_{\text{ham}}^{\text{ham}} F_{\text{ham}}(t_s)$$
$$+ \left\{ k_p^{\text{ham}}(\phi_{\text{trunk}}(t_s) - \phi_{\text{ref}}) + k_d^{\text{ham}} \dot{\phi}_{\text{trunk}}(t_s) \right\}_+ \tag{3.17}$$

where the third term returns the positive reflex contribution from the trunk balance control.

The full set of stance reflexes are:

$$S^{\text{sol}}(t) = S_0^{\text{sol}} + G_{\text{sol}}^{\text{sol}} F_{\text{sol}}(t_1) \tag{3.18}$$

$$S^{\text{ta}}(t) = S_0^{\text{ta}} + G_{\text{ta}}^{\text{ta}} \left(l_{\text{CE,ta}}(t_1) - l_{\text{ta}}^{\text{off}} \right) - G_{\text{sol}}^{\text{ta}} F_{\text{sol}}(t_1) \tag{3.19}$$

$$S^{\text{gas}}(t) = S_0^{\text{gas}} + G_{\text{gas}}^{\text{gas}} F_{\text{gas}}(t_1) \tag{3.20}$$

$$S^{\text{vas}}(t) = S_0^{\text{vas}} + G_{\text{vas}}^{\text{vas}} F_{\text{vas}}(t_{\text{m}}) - k_\phi \left(\phi_{\text{k}}(t_{\text{m}}) - \phi_{\text{k}}^{\text{off}} \right) \left(\phi_{\text{k}}(t_{\text{m}}) < \phi_{\text{k}}^{\text{off}} \right) (\dot{\phi}_{\text{k}}(t_{\text{m}}) < 0) \tag{3.21}$$

$$S^{\text{ham}}(t) = S_0^{\text{ham}} + G_{\text{ham}}^{\text{ham}} F_{\text{ham}}(t_s) + \left\{ k_{\text{p}}^{\text{ham}}(\phi_{\text{trunk}} - \phi_{\text{ref}}) + k_{\text{d}}^{\text{ham}} \dot{\phi}_{\text{trunk}} \right\}_+ \tag{3.22}$$

$$S^{\text{glu}}(t) = S_0^{\text{glu}} + G_{\text{glu}}^{\text{glu}} F_{\text{glu}}(t_s) + \left\{ k_{\text{p}}^{\text{glu}}(\phi_{\text{trunk}} - \phi_{\text{ref}}) + k_{\text{d}}^{\text{glu}} \dot{\phi}_{\text{trunk}} \right\}_- \tag{3.23}$$

$$S^{\text{hfl}}(t) = S_0^{\text{hfl}} + \left\{ k_{\text{p}}^{\text{hfl}}(\phi_{\text{trunk}} - \phi_{\text{ref}}) + k_{\text{d}}^{\text{hfl}} \dot{\phi}_{\text{trunk}} \right\}_+ \tag{3.24}$$

3.4 Swing Leg Control

During swing, the reflexes shape the natural double pendulum dynamics of the leg in order to achieve sufficient knee flexion, prevent toe scuffing, reach a target landing leg angle, and then extend the leg towards the ground. We here review two versions of the swing leg contro: First, an idealized controal, proposed in Desai and Geyer [2012], which proposes reflexes that directly apply torques to the knee and ankle joints, and second, a muscle reflex control, presented in Desai and Geyer [2013], which applies neural stimulations to Hill-type muscles to achieve the functionality of the idealzed control.

3.4.1 Idealized Swing Leg Control

The idealized swing control comprises two layers. In the first layer, a leg placement policy

$$\alpha_{\text{tgt}} = \alpha_0 + c_{\text{d}} d + c_{\text{v}} v \tag{3.25}$$

prescribes desired foot placement locations, where α_{tgt} is the target leg angle, α_0 is the default leg angle, d is the horizontal distance between the stance leg ankle and the model's center of mass, v is the velocity of the center of mass, and c_{d} and c_{v} are constant gain parameters. This policy is taken from Yin et al. [2007] and represents an empirical generalization of the leg placement strategies that recover the linear inverted pendulum model of human walking from disturbances [Kajita et al., 2001, Pratt et al., 2006].

The target angle generated by this policy forms a central input to the second layer comprised of hip and knee controls. The portion of this control that governs the knee action uses a finite state machine to switch between three phases. The first phase allows the knee to passively flex in response to hip moments generated at the

onset of swing. If the passive knee flexion is insufficient (the foot swings forward with a tendency to scuff the ground), the control produces active flexion torque of the knee in proportion to the rate $\dot{\alpha}$ of forward leg motion,

$$\tau_k^i = \begin{cases} 0, & \dot{\alpha} > 0 \\ -k^i\dot{\alpha}, & \dot{\alpha} \leq 0 \end{cases}, \tag{3.26}$$

where k^i is the flexion gain and the leg angle α is defined as the angle between the horizontal and the hip-ankle line.

The second phase activates when the leg length, defined as the distance between the hip and ankle, contracts below a threshold. In this phase, the knee torque is given by

$$\tau_k^{ii} = \begin{cases} -k_1^{ii}\dot{\phi}_k, & \dot{\phi}_k \geq 0 \\ -k_2^{ii}\dot{\phi}_k(\alpha - \alpha_{tgt})(\dot{\alpha} - \dot{\phi}_k), & \dot{\phi}_k < 0 \ \& \ \dot{\phi}_k < \dot{\alpha} , \\ 0, & \text{otherwise} \end{cases} \tag{3.27}$$

where k_1^{ii} and k_2^{ii} are damping coefficients. The first case dampens knee flexion, while the second case dampens knee extension, but allows progressively more extension as the leg angle approaches its target. The modulation term $(\dot{\alpha} - \dot{\phi}_k)$ prevents premature landing of the leg by damping the knee if it extends faster than the overall leg angle.

The third phase engages when the leg angle gets within a threshold of the target leg angle. The control then applies torque to stop and extend the knee,

$$\tau_k^{iii} = \begin{cases} k^{iii}(\alpha_{thr} - \alpha)\left(1 - \frac{\dot{\alpha}}{\dot{\alpha}_{max}}\right), & \alpha < \alpha_{thr} \ \& \ \dot{\alpha} < \dot{\alpha}_{max} \\ 0, & \text{otherwise} \end{cases}, \tag{3.28}$$

where $\dot{\alpha}_{max}$ is the maximum leg retraction velocity for which the stopping knee torque is applied. When this torque brings the leg velocity to zero, a knee extension torque is added,

$$\tau_k^{iii'} = \tau_k^{iii} - k^{ext}(l_0 - l), \tag{3.29}$$

where l_0 is the rest leg length, l is the current leg length, and k^{ext} is a proportional gain.

The swing leg control also specifies a hip torque in the form of a proportional derivative control on the leg angle,

$$\tau_h^\alpha = k_p(\alpha_{tgt} - \alpha) - k_d\dot{\alpha}. \tag{3.30}$$

This hip torque is supplemented by a feed forward term

$$\tau_h = \tau_h^\alpha - 2\tau_k^{iii} \tag{3.31}$$

that neutralizes the coupling dynamics between the knee and hip during the knee's stop and extend phase (Eq. 3.28).

The torques produced by the swing controller augment the net torques produced by the Hill-type muscles and reflexes during stance. At heel strike, the control policy switches from using the swing leg control torques to the stance torques generated by the muscle models. In late stance, the policy mixes the torques specified by the stance and swing controllers by scaling the stance and swing torques and muscle stimulations in proportion to the normalized ground reaction force,

$$\tau_{\text{late stance}} = \tau_{\text{stance}}(GRF) + \tau_{\text{swing}}(1 - GRF), \qquad (3.32)$$
$$S^m_{\text{late stance}} = S^m(GRF). \qquad (3.33)$$

During swing, only the swing leg torques are used.

3.4.2 *Neuromuscular Reflex Swing Leg Control*

4
Completed Work

5
Proposed Work

Bibliography

Brenna D Argall, Sonia Chernova, Manuela Veloso, and Brett Browning. A survey of robot learning from demonstration. *Robotics and autonomous systems*, 57(5):469–483, 2009.

Samuel K Au and Hugh M Herr. Powered ankle-foot prosthesis. *IEEE Robotics & Automation Magazine*, 15(3):52–59, 2008.

Samuel K Au, Jeff Weber, and Hugh Herr. Biomechanical design of a powered ankle-foot prosthesis. In *2007 IEEE 10th International conference on rehabilitation robotics*, pages 298–303. IEEE, 2007.

Ryan D Bellman, Matthew A Holgate, and Thomas G Sugar. Sparky 3: Design of an active robotic ankle prosthesis with two actuated degrees of freedom using regenerative kinetics. In *2008 2nd IEEE RAS & EMBS International Conference on Biomedical Robotics and Biomechatronics*, pages 511–516. IEEE, 2008.

Malte Bellmann, Thomas Schmalz, and Siegmar Blumentritt. Comparative biomechanical analysis of current microprocessor-controlled prosthetic knee joints. *Archives of physical medicine and rehabilitation*, 91(4):644–652, 2010.

T Graham Brown. The intrinsic factors in the act of progression in the mammal. *Proceedings of the Royal Society of London. Series B, containing papers of a biological character*, 84(572):308–319, 1911.

Frank L Buczek and PETER R Cavanagh. Stance phase knee and ankle kinematics and kinetics during level and downhill running. *Med Sci Sports Exerc*, 22(5):669–677, 1990.

Etienne Burdet, Rieko Osu, David W Franklin, Theodore E Milner, and Mitsuo Kawato. The central nervous system stabilizes unstable dynamics by learning optimal impedance. *Nature*, 414(6862):446–449, 2001.

Jean-Marie Cabelguen, Céline Bourcier-Lucas, and Réjean Dubuc. Bimodal locomotion elicited by electrical stimulation of the mid-

brain in the salamander notophthalmus viridescens. *The Journal of Neuroscience*, 23(6):2434–2439, 2003.

C Capaday and RB Stein. Difference in the amplitude of the human soleus h reflex during walking and running. *The Journal of physiology*, 392:513, 1987.

Charles Capaday. The special nature of human walking and its neural control. *Trends in neurosciences*, 25(7):370–376, 2002.

Joshua M Caputo and Steven H Collins. An experimental robotic testbed for accelerated development of ankle prostheses. In *Robotics and automation (ICRA), 2013 IEEE international conference on*, pages 2645–2650. IEEE, 2013.

Joshua M Caputo, Peter G Adamczyk, and Steven H Collins. Informing ankle-foot prosthesis prescription through haptic emulation of candidate devices. In *2015 IEEE International Conference on Robotics and Automation (ICRA)*, pages 6445–6450. IEEE, 2015.

Avis H Cohen and P Wallén. The neuronal correlate of locomotion in fish. *Experimental brain research*, 41(1):11–18, 1980.

Steve Collins, Andy Ruina, Russ Tedrake, and Martijn Wisse. Efficient bipedal robots based on passive-dynamic walkers. *Science*, 307(5712): 1082–1085, 2005.

A Forner Cordero, HJFM Koopman, and Frans CT van der Helm. Energy analysis of human stumbling: the limitations of recovery. *Gait & posture*, 21(3):243–254, 2005.

DT Davy and ML Audu. A dynamic optimization technique for predicting muscle forces in the swing phase of gait. *Journal of biomechanics*, 20(2):187–201, 1987.

Isabelle Delvolvé, Pascal Branchereau, Réjean Dubuc, and Jean-Marie Cabelguen. Fictive rhythmic motor patterns induced by nmda in an in vitro brain stem–spinal cord preparation from an adult urodele. *Journal of Neurophysiology*, 82(2):1074–1077, 1999.

Ruta Desai and Hartmut Geyer. Robust swing leg placement under large disturbances. In *Robotics and Biomimetics (ROBIO), 2012 IEEE International Conference on*, pages 265–270. IEEE, 2012.

Ruta Desai and Hartmut Geyer. Muscle-reflex control of robust swing leg placement. In *Robotics and Automation (ICRA), 2013 IEEE International Conference on*, pages 2169–2174. IEEE, 2013.

Max Donath. *Proportional EMG control for above knee pros-theses*. PhD thesis, Massachusetts Institute of Technology, 1974.

Michael F Eilenberg, Hartmut Geyer, and Hugh Herr. Control of a powered ankle–foot prosthesis based on a neuromuscular model. *Neural Systems and Rehabilitation Engineering, IEEE Transactions on*, 18(2):164–173, 2010.

Gen Endo, Jun Nakanishi, Jun Morimoto, and Gordon Cheng. Experimental studies of a neural oscillator for biped locomotion with qrio. In *Proceedings of the 2005 IEEE international conference on robotics and automation*, pages 596–602. IEEE, 2005.

Janice J Eng, David A Winter, and Aftab E Patla. Strategies for recovery from a trip in early and late swing during human walking. *Experimental Brain Research*, 102(2):339–349, 1994.

Johannes Englsberger, Twan Koolen, Sylvain Bertrand, Jerry Pratt, Christian Ott, and Alin Albu-Schäffer. Trajectory generation for continuous leg forces during double support and heel-to-toe shift based on divergent component of motion. In *2014 IEEE/RSJ International Conference on Intelligent Robots and Systems*, pages 4022–4029. IEEE, 2014.

Siyuan Feng, Eric Whitman, X Xinjilefu, and Christopher G Atkeson. Optimization-based full body control for the darpa robotics challenge. *Journal of Field Robotics*, 32(2):293–312, 2015.

Woodie C Flowers. Use of an amputee-computer interactive facility in above-knee prosthesis research. In *Proceedings of the 1974 annual conference-Volume 1*, pages 335–339. ACM, 1974.

Christiane Gauthier-Gagnon, Marie-Claude Grisé, and Diane Potvin. Enabling factors related to prosthetic use by people with transtibial and transfemoral amputation. *Archives of physical medicine and rehabilitation*, 80(6):706–713, 1999.

Yanli Geng, Peng Yang, Xiaoyun Xu, and Lingling Chen. Design and simulation of active transfemoral prosthesis. In *2012 24th Chinese Control and Decision Conference (CCDC)*, pages 3724–3728. IEEE, 2012.

Hartmut Geyer and Hugh Herr. A muscle-reflex model that encodes principles of legged mechanics produces human walking dynamics and muscle activities. *IEEE Transactions on neural systems and rehabilitation engineering*, 18(3):263–273, 2010.

Hartmut Geyer, Andre Seyfarth, and Reinhard Blickhan. Compliant leg behaviour explains basic dynamics of walking and running. *Proceedings of the Royal Society of London B: Biological Sciences*, 273 (1603):2861–2867, 2006.

Robert D Gregg, Tommaso Lenzi, Levi J Hargrove, and Jonathon W Sensinger. Virtual constraint control of a powered prosthetic leg: From simulation to experiments with transfemoral amputees. *IEEE Transactions on Robotics*, 30(6):1455–1471, 2014.

Michael J Grey, Jens Bo Nielsen, Nazarena Mazzaro, and Thomas Sinkjær. Positive force feedback in human walking. *The Journal of physiology*, 581(1):99–105, 2007.

DL Grimes, WC Flowers, and M Donath. Feasibility of an active control scheme for above knee prostheses. *Journal of Biomechanical Engineering*, 99(4):215–221, 1977.

Donald Lee Grimes. *An active multi-mode above knee prosthesis controller*. PhD thesis, Massachusetts Institute of Technology, 1979.

Jesse A Grimes. *ATRIAS 1.0 & 2.1: enabling agile biped locomotion with a template-driven approach to robot design*. PhD thesis, Oregon State University, 2013.

Michael Günther and Hanns Ruder. Synthesis of two-dimensional human walking: a test of the λ-model. *Biological cybernetics*, 89(2): 89–106, 2003.

Xin Guo, Lingling Chen, Yang Zhang, Peng Yang, and Liqun Zhang. A study on control mechanism of above knee robotic prosthesis based on cpg model. In *Robotics and Biomimetics (ROBIO), 2010 IEEE International Conference on*, pages 283–287. IEEE, 2010.

Kevin H Ha, Huseyin Atakan Varol, and Michael Goldfarb. Volitional control of a prosthetic knee using surface electromyography. *IEEE Transactions on Biomedical Engineering*, 58(1):144–151, 2011.

Levi J Hargrove, Aaron J Young, Ann M Simon, Nicholas P Fey, Robert D Lipschutz, Suzanne B Finucane, Elizabeth G Halsne, Kimberly A Ingraham, and Todd A Kuiken. Intuitive control of a powered prosthetic leg during ambulation: a randomized clinical trial. *JAMA*, 313(22):2244–2252, 2015.

Hugh M. Herr and Alena M. Grabowski. Bionic ankle–foot prosthesis normalizes walking gait for persons with leg amputation. *Proceedings of the Royal Society of London B: Biological Sciences*, 279(1728):457–464, 2011. ISSN 0962-8452. DOI: 10.1098/rspb.2011.1194. URL http://rspb.royalsocietypublishing.org/content/279/1728/457.

Alexander Herzog, Ludovic Righetti, Felix Grimminger, Peter Pastor, and Stefan Schaal. Balancing experiments on a torque-controlled humanoid with hierarchical inverse dynamics. In *2014 IEEE/RSJ*

International Conference on Intelligent Robots and Systems, pages 981–988. IEEE, 2014.

Kazuo Hirai, Masato Hirose, Yuji Haikawa, and Toru Takenaka. The development of honda humanoid robot. In *Robotics and Automation, 1998. Proceedings. 1998 IEEE International Conference on*, volume 2, pages 1321–1326. IEEE, 1998.

Joseph K Hitt, Ryan Bellman, Matthew Holgate, Thomas G Sugar, and Kevin W Hollander. The sparky (spring ankle with regenerative kinetics) project: Design and analysis of a robotic transtibial prosthesis with regenerative kinetics. In *ASME 2007 International Design Engineering Technical Conferences and Computers and Information in Engineering Conference*, pages 1587–1596. American Society of Mechanical Engineers, 2007.

Cheriel J Hofstad, Vivian Weerdesteyn, Harmen van der Linde, Bart Nienhuis, Alexander C Geurts, and Jacques Duysens. Evidence for bilaterally delayed and decreased obstacle avoidance responses while walking with a lower limb prosthesis. *Clinical Neurophysiology*, 120(5):1009–1015, 2009.

Neville Hogan. Impedance control: An approach to manipulation: Part ii—implementation. *Journal of dynamic systems, measurement, and control*, 107(1):8–16, 1985.

Matthew A Holgate, Joseph K Hitt, Ryan D Bellman, Thomas G Sugar, and Kevin W Hollander. The sparky (spring ankle with regenerative kinetics) project: Choosing a dc motor based actuation method. In *2008 2nd IEEE RAS & EMBS International Conference on Biomedical Robotics and Biomechatronics*, pages 163–168. IEEE, 2008.

He Huang, Todd A Kuiken, Robert D Lipschutz, et al. A strategy for identifying locomotion modes using surface electromyography. *IEEE Transactions on Biomedical Engineering*, 56(1):65–73, 2009.

He Huang, Fan Zhang, Levi J Hargrove, Zhi Dou, Daniel R Rogers, and Kevin B Englehart. Continuous locomotion-mode identification for prosthetic legs based on neuromuscular–mechanical fusion. *IEEE Transactions on Biomedical Engineering*, 58(10):2867–2875, 2011.

CL Hubley and RP Wells. A work-energy approach to determine individual joint contributions to vertical jump performance. *European Journal of Applied Physiology and Occupational Physiology*, 50(2): 247–254, 1983.

Amanda M Huff, Brian E Lawson, and Michael Goldfarb. A running controller for a powered transfemoral prosthesis. In *2012 Annual*

International Conference of the IEEE Engineering in Medicine and Biology Society, pages 4168–4171. IEEE, 2012.

Marco Hutter, Mark A Hoepflinger, Christian Gehring, Michael Bloesch, C David Remy, and Roland Siegwart. Hybrid operational space control for compliant legged systems. *Robotics: Science and systems VIII*, page 129, 2013.

Auke Jan Ijspeert. Central pattern generators for locomotion control in animals and robots: a review. *Neural Networks*, 21(4):642–653, 2008.

Sonja MHJ Jaegers, J Hans Arendzen, and Henry J de Jongh. Prosthetic gait of unilateral transfemoral amputees: a kinematic study. *Archives of physical medicine and rehabilitation*, 76(8):736–743, 1995.

Jennifer L Johansson, Delsey M Sherrill, Patrick O Riley, Paolo Bonato, and Hugh Herr. A clinical comparison of variable-damping and mechanically passive prosthetic knee devices. *American journal of physical medicine & rehabilitation*, 84(8):563–575, 2005.

Shuuji Kajita and Kazuo Tani. Study of dynamic biped locomotion on rugged terrain-derivation and application of the linear inverted pendulum mode. In *Robotics and Automation, 1991. Proceedings., 1991 IEEE International Conference on*, pages 1405–1411. IEEE, 1991.

Shuuji Kajita, Fumio Kanehiro, Kenji Kaneko, Kazuhito Yokoi, and Hirohisa Hirukawa. The 3d linear inverted pendulum mode: A simple modeling for a biped walking pattern generation. In *Intelligent Robots and Systems, 2001. Proceedings. 2001 IEEE/RSJ International Conference on*, volume 1, pages 239–246. IEEE, 2001.

Shuuji Kajita, Fumio Kanehiro, Kenji Kaneko, Kiyoshi Fujiwara, Kensuke Harada, Kazuhito Yokoi, and Hirohisa Hirukawa. Biped walking pattern generation by using preview control of zero-moment point. In *Robotics and Automation, 2003. Proceedings. ICRA'03. IEEE International Conference on*, volume 2, pages 1620–1626. IEEE, 2003.

Shuuji Kajita, Takashi Nagasaki, Kenji Kaneko, and Hirohisa Hirukawa. Zmp-based biped running control. *IEEE robotics & automation magazine*, 2(14):63–72, 2007.

Robert E Kearney and Ian W Hunter. System identification of human joint dynamics. *Critical reviews in biomedical engineering*, 18(1):55–87, 1989.

Scott Kuindersma, Frank Permenter, and Russ Tedrake. An efficiently solvable quadratic program for stabilizing dynamic locomotion. In

2014 IEEE International Conference on Robotics and Automation (ICRA), pages 2589–2594. IEEE, 2014.

Brian E Lawson, H Atakan Varol, Frank Sup, and Michael Goldfarb. Stumble detection and classification for an intelligent transfemoral prosthesis. In *2010 Annual International Conference of the IEEE Engineering in Medicine and Biology*, pages 511–514. IEEE, 2010.

Brian E Lawson, Jason Mitchell, Don Truex, Amanda Shultz, Elissa Ledoux, and Michael Goldfarb. A robotic leg prosthesis: Design, control, and implementation. *IEEE Robotics & Automation Magazine*, 21(4):70–81, 2014.

Brian Edward Lawson, Huseyin Atakan Varol, Amanda Huff, Erdem Erdemir, and Michael Goldfarb. Control of stair ascent and descent with a powered transfemoral prosthesis. *IEEE Transactions on Neural Systems and Rehabilitation Engineering*, 21(3):466–473, 2013.

T Lenzi, LJ Hargrove, and JW Sensinger. Minimum jerk swing control allows variable cadence in powered transfemoral prostheses. In *Conference Proceedings IEEE Engineering in Medicine and Biology Society*, pages 2492–2495, 2014a.

Tommaso Lenzi, Levi Hargrove, and Jonathon Sensinger. Speed-adaptation mechanism: Robotic prostheses can actively regulate joint torque. *IEEE Robotics & Automation Magazine*, 21(4):94–107, 2014b.

David R Lide. *CRC handbook of chemistry and physics*, volume 85. CRC press, 2004.

Marilyn MacKay-Lyons. Central pattern generation of locomotion: a review of the evidence. *Physical therapy*, 82(1):69–83, 2002.

Jared Markowitz, Pavitra Krishnaswamy, Michael F Eilenberg, Ken Endo, Chris Barnhart, and Hugh Herr. Speed adaptation in a powered transtibial prosthesis controlled with a neuromuscular model. *Philosophical Transactions of the Royal Society of London B: Biological Sciences*, 366(1570):1621–1631, 2011.

William C Martin, Albert Wu, and Hartmut Geyer. Robust spring mass model running for a physical bipedal robot. In *2015 IEEE International Conference on Robotics and Automation (ICRA)*, pages 6307–6312. IEEE, 2015.

Ernesto C Martinez-Villalpando, Jeff Weber, Grant Elliott, and Hugh Herr. Design of an agonist-antagonist active knee prosthesis. In *2008 2nd IEEE RAS & EMBS International Conference on Biomedical Robotics and Biomechatronics*, pages 529–534. IEEE, 2008.

Ernesto C Martinez-Villalpando, Luke Mooney, Grant Elliott, and Hugh Herr. Antagonistic active knee prosthesis. a metabolic cost of walking comparison with a variable-damping prosthetic knee. In *2011 Annual International Conference of the IEEE Engineering in Medicine and Biology Society*, pages 8519–8522. IEEE, 2011.

Kiyotoshi Matsuoka. Mechanisms of frequency and pattern control in the neural rhythm generators. *Biological cybernetics*, 56(5-6):345–353, 1987.

ANDREW D McClellan and WOOCHAN Jang. Mechanosensory inputs to the central pattern generators for locomotion in the lamprey spinal cord: resetting, entrainment, and computer modeling. *Journal of Neurophysiology*, 70(6):2442–2454, 1993.

Tad McGeer. Passive dynamic walking. *The international journal of robotics research*, 9(2):62–82, 1990.

William C Miller, Mark Speechley, and Barry Deathe. The prevalence and risk factors of falling and fear of falling among lower extremity amputees. *Archives of physical medicine and rehabilitation*, 82(8): 1031–1037, 2001.

Simon Mochon and Thomas A McMahon. Ballistic walking. *Journal of biomechanics*, 13(1):49–57, 1980.

Gaspar Mora, Rafael R Torrealba, José Cappelletto, Leonardo Fermín, G Fernández-López, and Juan C Grieco. Cybernetic knee prosthesis: application of an adaptive central pattern generator. *Kybernetes*, 41 (1/2):192–205, 2012.

Maxon Motor. Mason ec-4pole, Apr 2016a. URL `http://www. maxonmotorusa.com/medias/sys_master/root/8821066268702/ 16-274-en.pdf`.

Maxon Motor. Maxon flat motor, Apr 2016b. URL `http://www. maxonmotorusa.com/medias/sys_master/root/8821068005406/ 16-304-en.pdf`.

Akihiko Murai and Katsu Yamane. A neuromuscular locomotion controller that realizes human-like responses to unexpected disturbances. In *Robotics and Automation (ICRA), 2011 IEEE International Conference on*, pages 1997–2002. IEEE, 2011.

Sylvie Nadeau, Bradford J McFadyen, and Francine Malouin. Frontal and sagittal plane analyses of the stair climbing task in healthy adults aged over 40 years: what are the challenges compared to level walking? *Clinical Biomechanics*, 18(10):950–959, 2003.

Gora Chand Nandi, Auke Jan Ijspeert, Pavan Chakraborty, and Anirban Nandi. Development of adaptive modular active leg (amal) using bipedal robotics technology. *Robotics and Autonomous Systems*, 57(6):603–616, 2009.

Jens Bo Nielsen. How we walk: central control of muscle activity during human walking. *The Neuroscientist*, 9(3):195–204, 2003.

Naomichi Ogihara and Nobutoshi Yamazaki. Generation of human bipedal locomotion by a bio-mimetic neuro-musculo-skeletal model. *Biological cybernetics*, 84(1):1–11, 2001.

Jacquelin Perry and Judith M Burnfield. *Gait analysis: normal and pathological function*. Slack Thorofare, NJ, 1992.

Michael Raymond Pierrynowski and James Barbour Morrison. A physiological model for the evaluation of muscular forces in human locomotion: theoretical aspects. *Mathematical Biosciences*, 75(1): 69–101, 1985.

Mirjam Pijnappels, Maarten F Bobbert, and Jaap H van Dieën. Contribution of the support limb in control of angular momentum after tripping. *Journal of biomechanics*, 37(12):1811–1818, 2004.

Gill A Pratt and Matthew M Williamson. Series elastic actuators. In *Intelligent Robots and Systems 95.'Human Robot Interaction and Cooperative Robots', Proceedings. 1995 IEEE/RSJ International Conference on*, volume 1, pages 399–406. IEEE, 1995.

Jerry Pratt and Ben Krupp. Design of a bipedal walking robot. In *SPIE defense and security symposium*, pages 69621F–69621F. International Society for Optics and Photonics, 2008.

Jerry Pratt, Chee-Meng Chew, Ann Torres, Peter Dilworth, and Gill Pratt. Virtual model control: An intuitive approach for bipedal locomotion. *The International Journal of Robotics Research*, 20(2): 129–143, 2001.

Jerry Pratt, John Carff, Sergey Drakunov, and Ambarish Goswami. Capture point: A step toward humanoid push recovery. In *2006 6th IEEE-RAS international conference on humanoid robots*, pages 200–207. IEEE, 2006.

Marc Harold Raibert, H Benjamin Brown, Michael Chepponis, and Eugene Hastings. Dynamically stable legged locomotion: second report to darpa, october 1, 1981-december 31, 1982. Technical report, Carnegie Mellon University, 1983.

Jack Alan Rall. Energetic aspects of skeletal muscle contraction: implications of fiber types. *Exercise and sport sciences reviews*, 13: 33–74, 1984.

Ludovic Righetti and Auke Jan Ijspeert. Programmable central pattern generators: an application to biped locomotion control. In *Proceedings 2006 IEEE International Conference on Robotics and Automation, 2006. ICRA 2006.*, pages 1585–1590. IEEE, 2006.

Ludovic Righetti, Jonas Buchli, and Auke Jan Ijspeert. Dynamic hebbian learning in adaptive frequency oscillators. *Physica D: Nonlinear Phenomena*, 216(2):269–281, 2006.

David William Robinson. *Design and analysis of series elasticity in closed-loop actuator force control*. PhD thesis, Massachusetts Institute of Technology, 2000.

Stéphane Ross, Geoffrey J Gordon, and Drew Bagnell. A reduction of imitation learning and structured prediction to no-regret online learning. In *AISTATS*, page 6, 2011.

Serge Rossignol. Locomotion and its recovery after spinal injury. *Current opinion in neurobiology*, 10(6):708–716, 2000.

Elliott J Rouse, Robert D Gregg, Levi J Hargrove, and Jonathon W Sensinger. The difference between stiffness and quasi-stiffness in the context of biomechanical modeling. *IEEE Transactions on Biomedical Engineering*, 60(2):562–568, 2013.

Elliott J Rouse, Luke M Mooney, and Hugh M Herr. Clutchable series-elastic actuator: Implications for prosthetic knee design. *The International Journal of Robotics Research*, page 0278364914545673, 2014.

Elliott J Rouse, Nathan C Villagaray-Carski, Robert W Emerson, and Hugh M Herr. Design and testing of a bionic dancing prosthesis. *PloS one*, 10(8):e0135148, 2015.

Layale Saab, Oscar E Ramos, François Keith, Nicolas Mansard, Philippe Soueres, and Jean-Yves Fourquet. Dynamic whole-body motion generation under rigid contacts and other unilateral constraints. *IEEE Transactions on Robotics*, 29(2):346–362, 2013.

Gregory S Sawicki, Cara L Lewis, and Daniel P Ferris. It pays to have a spring in your step. *Exercise and sport sciences reviews*, 37(3):130, 2009.

Alexander Schepelmann. *Evaluation of Decentralized Reactive Swing-Leg Controllers on Powered Robotic Legs*. PhD thesis, Carnegie Mellon University, 2016.

AM Schillings, BMH Van Wezel, TH Mulder, and Jaak Duysens. Muscular responses and movement strategies during stumbling over obstacles. *Journal of Neurophysiology*, 83(4):2093–2102, 2000.

Stephen H Scott and David A Winter. Biomechanical model of the human foot: kinematics and kinetics during the stance phase of walking. *Journal of biomechanics*, 26(9):1091–1104, 1993.

Jiang Shan and Fumio Nagashima. Neural locomotion controller design and implementation for humanoid robot hoap-1. In *20th annual conference of the robotics society of Japan*, 2002.

Charles Sherrington. *The integrative action of the nervous system*. CUP Archive, 1910a.

Charles Scott Sherrington. Flexion-reflex of the limb, crossed extension-reflex, and reflex stepping and standing. *The Journal of physiology*, 40 (1-2):28–121, 1910b.

ML Shik, FV Severin, and ORLOVSKI. GN. Control of walking and running by means of electrical stimulation of mid-brain. *BIOPHYSICS-USSR*, 11(4):756, 1966.

Shuhei Shimmyo, Tomoya Sato, and Kouhei Ohnishi. Biped walking pattern generation by using preview control with virtual plane method. In *2010 11th IEEE International Workshop on Advanced Motion Control (AMC)*, pages 414–419. IEEE, 2010.

Camila Shirota, Ann M Simon, and Todd A Kuiken. Recovery strategy identification throughout swing phase using kinematic data from the tripped leg. In *2014 36th Annual International Conference of the IEEE Engineering in Medicine and Biology Society*, pages 6199–6202. IEEE, 2014.

Camila Shirota, Ann M Simon, and Todd A Kuiken. Transfemoral amputee recovery strategies following trips to their sound and prosthesis sides throughout swing phase. *Journal of neuroengineering and rehabilitation*, 12(1):1, 2015.

Amanda H Shultz, Jason E Mitchell, Don Truex, Brian E Lawson, Elissa Ledoux, and Michael Goldfarb. A walking controller for a powered ankle prosthesis. In *2014 36th Annual International Conference of the IEEE Engineering in Medicine and Biology Society*, pages 6203–6206. IEEE, 2014.

Amanda H Shultz, Brian E Lawson, and Michael Goldfarb. Running with a powered knee and ankle prosthesis. *IEEE Transactions on Neural Systems and Rehabilitation Engineering*, 23(3):403–412, 2015.

SR Soffe and Alan Roberts. Tonic and phasic synaptic input to spinal cord motoneurons during fictive locomotion in frog embryos. *Journal of Neurophysiology*, 48(6):1279–1288, 1982.

Seungmoon Song and Hartmut Geyer. Generalization of a muscle-reflex control model to 3d walking. In *2013 35th Annual International Conference of the IEEE Engineering in Medicine and Biology Society (EMBC)*, pages 7463–7466. IEEE, 2013.

Seungmoon Song and Hartmut Geyer. A neural circuitry that emphasizes spinal feedback generates diverse behaviours of human locomotion. *The Journal of physiology*, 593(16):3493–3511, 2015.

Seungmoon Song, Ruta Desai, and Hartmut Geyer. Integration of an adaptive swing control into a neuromuscular human walking model. In *2013 35th Annual International Conference of the IEEE Engineering in Medicine and Biology Society (EMBC)*, pages 4915–4918. IEEE, 2013.

Koushil Sreenath, Hae-Won Park, Ioannis Poulakakis, and Jessy W Grizzle. A compliant hybrid zero dynamics controller for stable, efficient and fast bipedal walking on mabel. *The International Journal of Robotics Research*, 30(9):1170–1193, 2011.

JE Stewart, H Barbeau, and S Gauthier. Modulation of locomotor patterns and spasticity with clonidine in spinal cord injured patients. *Canadian Journal of Neurological Sciences/Journal Canadien des Sciences Neurologiques*, 18(03):321–332, 1991.

Frank Sup, Amit Bohara, and Michael Goldfarb. Design and control of a powered knee and ankle prosthesis. In *Proceedings 2007 IEEE International Conference on Robotics and Automation*, pages 4134–4139. IEEE, 2007.

Frank Sup, Amit Bohara, and Michael Goldfarb. Design and control of a powered transfemoral prosthesis. *The International journal of robotics research*, 27(2):263–273, 2008.

Frank Sup, Huseyin Atakan Varol, Jason Mitchell, Thomas J Withrow, and Michael Goldfarb. Preliminary evaluations of a self-contained anthropomorphic transfemoral prosthesis. *IEEE/ASME Transactions on mechatronics*, 14(6):667–676, 2009.

Frank Sup, Huseyin Atakan Varol, and Michael Goldfarb. Upslope walking with a powered knee and ankle prosthesis: initial results with an amputee subject. *IEEE Transactions on Neural Systems and Rehabilitation Engineering*, 19(1):71–78, 2011.

Gentaro Taga, Yoko Yamaguchi, and Hiroshi Shimizu. Self-organized control of bipedal locomotion by neural oscillators in unpredictable environment. *Biological cybernetics*, 65(3):147–159, 1991.

Nitish Thatte and Hartmut Geyer. Toward balance recovery with leg prostheses using neuromuscular model control. *IEEE Transactions on Biomedical Engineering*, 63(5):904–913, 2016.

Rafael R Torrealba, Claudia Pérez-D'Arpino, José Cappelletto, Leonardo Fermin-Leon, Gerardo Fernández-López, and Juan C Grieco. Through the development of a biomechatronic knee prosthesis for transfemoral amputees: mechanical design and manufacture, human gait characterization, intelligent control strategies and tests. In *Robotics and Automation (ICRA), 2010 IEEE International Conference on*, pages 2934–2939. IEEE, 2010.

Huseyin Atakan Varol, Frank Sup, and Michael Goldfarb. Powered sit-to-stand and assistive stand-to-sit framework for a powered transfemoral prosthesis. In *2009 IEEE International Conference on Rehabilitation Robotics*, pages 645–651. IEEE, 2009.

Huseyin Atakan Varol, Frank Sup, and Michael Goldfarb. Multiclass real-time intent recognition of a powered lower limb prosthesis. *IEEE Transactions on Biomedical Engineering*, 57(3):542–551, 2010.

Christopher L Vaughan. Theories of bipedal walking: an odyssey. *Journal of biomechanics*, 36(4):513–523, 2003.

Jing Wang, Oliver A Kannape, and Hugh M Herr. Proportional emg control of ankle plantar flexion in a powered transtibial prosthesis. In *Rehabilitation Robotics (ICORR), 2013 IEEE International Conference on*, pages 1–5. IEEE, 2013.

RL Waters, Jacquelin Perry, DANIEL Antonelli, and Helen Hislop. Energy cost of walking of amputees: the influence of level of amputation. *J Bone Joint Surg Am*, 58(1):42–46, 1976.

Patrick M Wensing and David E Orin. Generation of dynamic humanoid behaviors through task-space control with conic optimization. In *Robotics and Automation (ICRA), 2013 IEEE International Conference on*, pages 3103–3109. IEEE, 2013.

David A Winter. *Biomechanics and motor control of human movement*. John Wiley & Sons, 2009.

Justin Won and Neville Hogan. Stability properties of human reaching movements. *Experimental Brain Research*, 107(1):125–136, 1995.

Sai-Kit Wu, Garrett Waycaster, and Xiangrong Shen. Electromyography-based control of active above-knee prostheses. *Control Engineering Practice*, 19(8):875–882, 2011.

JAYNIE F Yang and RICHARD B Stein. Phase-dependent reflex reversal in human leg muscles during walking. *Journal of Neurophysiology*, 63(5):1109–1117, 1990.

JF Yang, RB Stein, and KB James. Contribution of peripheral afferents to the activation of the soleus muscle during walking in humans. *Experimental Brain Research*, 87(3):679–687, 1991.

KangKang Yin, Kevin Loken, and Michiel van de Panne. Simbicon: Simple biped locomotion control. In *ACM Transactions on Graphics (TOG)*, volume 26, page 105. ACM, 2007.

Fan Zhang, Susan E D'Andrea, Michael J Nunnery, Steven M Kay, and He Huang. Towards design of a stumble detection system for artificial legs. *IEEE Transactions on Neural Systems and Rehabilitation Engineering*, 19(5):567–577, 2011.

Huihua Zhao, Jonathan Horn, Jacob Reher, Victor Paredes, and Aaron D Ames. First steps toward translating robotic walking to prostheses: a nonlinear optimization based control approach. *Autonomous Robots*, pages 1–18, 2016.

Kathryn Ziegler-Graham, Ellen J MacKenzie, Patti L Ephraim, Thomas G Travison, and Ron Brookmeyer. Estimating the prevalence of limb loss in the united states: 2005 to 2050. *Archives of physical medicine and rehabilitation*, 89(3):422–429, 2008.